Chapter 2

DC Microgrid energy management with correlated uncertainties

2.1 Introduction

Growing electricity demand and concerns related to climate change have led to the integration of small-scale power generation units (called DG) and storage units near the customer site [1]. The concept of μG facilitates the integration of DG at the distribution level [129]. Presently, ACμGs are more popular. However, the development of PE-based devices has made DC systems accessible for broader applications. Sources such as SPG, WPG, BESS, and fuel cells generate the DC power. Also, modern loads such as laptops, mobile phones, and tablets require DC power to operate. The problems of frequency synchronisation and reactive power management do not arise in a DCμG. Therefore, a DCμG often provides a better solution for various residential and industrial applications [7]. The operation of a DCμG should be stable, economically viable, and meet the power quality requirements as per international standards. It is achieved by a well-designed EMS.

The power generated from renewable sources (SPG and WPG) are uncertain due to their dependency on climatic conditions [8]. Also, load demand and grid price are uncertain and cannot be taken as deterministic inputs. Further, the penetration of PHEV charging load has been increasing in recent years [130]. With the use of fast PHEV chargers, the problem of energy management becomes more complex. The degree of uncertainty on the generation and the demand side has increased with high penetration of uncertain RES and PHEV loads. The uncertainty increases the risk of the dispatch strategy since the

demand generation balance may not be satisfied with DGs of small ratings in a DCμG. Moreover, high RES generation or high load demands may cause bus voltage and line rating constraints to be violated, leading to cascaded failure. Techniques like "model predictive control", robust programming, stochastic programming, scenario-based approach, chance-constrained programming, etc., have been used to mitigate harmful impacts of RES generation and load demand uncertainties [44, 59, 131, 132, 133]. Moreover, the spatiotemporal complementarity of multi-energy sources like WPG and SPG and the coordinated scheduling of flexible resources can be used to reduce the volatility and improve the consumption of RES generation [59]. The concept of "integrated demand response" involves coordinating available flexibilities on the generation and load sides, like controllable power sources, ESS of different types (thermal, electrochemical, mechanical, etc.), flexible loads (shiftable and curtailable) to circumvent the volatility of RES generation and provide power bridging and ancillary services [44, 45, 59, 132]. Therefore, it is required to address the high penetration of DG and PHEVs along with the uncertainties (considering correlation) to design the EMS for a DCμG.

A literature survey on the EMS of a DCμG has been presented in **section 1.3**. A comparison of contributions made by relevant papers with the work done in this chapter is given in table 2.1. The following gap areas are found in the existing literature:

- **Gap#1)** Most researchers have not modelled the correlation between input RVs while formulating the EMS of a DCμG.

- **Gap#2)** Most Inverse NT based approaches for modelling correlation between input RVs used empirical relations to map correlation coefficients between the marginal distributions to the normal space. However, the empirical formulae are defined for only a few marginal distributions. Therefore, the above technique can be applied if the input RVs are modelled using marginal distributions for which empirical formulae have been defined. For instance, no empirical relationship is defined to map correlations between load (modelled using normal distribution) and wind speed (modelled by Weibull distribution). This limitation restricts the Inverse-NT-based approach to a few pdfs.

- **Gap#3)** The performance of a DCμG can be best optimised with proper coordination between power procurements from RES, implementation of DR program,

scheduling of BESS and DCSOPs. To the best of the author's knowledge, no reported EMS scheme on DCμG has encompassed all the above flexibility resources (see table 2.1).

The present chapter bridges the gap areas identified above by making the following contributions:

- **Contribution#1)** A MO EMS is formulated for a DCμG by modelling and incorporating uncertainties of RES, load demand, PHEV load, grid power price. The EMS strategy envisages coordination between power procurement from various sources (RES, grid, dispatchable unit), DR implementation, BESS and DCSOP scheduling. Therefore, the first and third gap areas are addressed.

- **Contribution#2)** Correlation between input RVs is modelled using an Inverse NT based approach. However, we have used Newton's Interpolation-based technique instead of empirical formulae for correlation mapping between normal space and arbitrary marginal distributions. Therefore, unlike the previously reported approaches, the proposed approach applies to any arbitrary marginal distribution. Hence, the second gap is bridged.

The remaining portions of the chapter are arranged into the following sections. Uncertainty modelling and mathematical models of the DCμG components are covered in **section 2.2**. The objective functions, constraints, and solution method are discussed in **section 2.3**. Simulation studies and results are presented in **section 2.4**. Conclusions are given in **section 2.5**.

2.2 System Modelling

Following assumptions are made in this study:

- Sufficient historical data is available for all the input RVs like, wind speed, load demand, grid energy price, the daily driven distance of PHEV, and smart charging behaviour of PHEV users. Therefore, the DCμGO can formulate pdfs to model uncertainties of all the input RVs.

Table 2.1: Summary of literature review

Ref.	Uncertainty Modelling			DR	BESS	DCSOP	Objective
	Entities	Correlation	Method				
[134]	✗	✗	NA	✗	✗	✗	Voltage profile improvement
[135]	✗	✗	NA	✗	✓	✗	Operational cost minimisation
[82]	✗	✗	NA	✗	✓	✗	Operational cost minimisation
[15]	✗	✗	NA	✗	✓	✗	Power balance control
[136]	✗	✗	NA	✗	✓	✗	Voltage profile improvement.
[137]	✗	✗	NA	✗	✓	✗	Voltage profile improvement
[16]	✗	✗	NA	✗	✓	✗	Cost reduction
[83]	✗	✗	NA	✗	✓	✗	Reliability improvement
[18]	✗	✗	NA	✓	✓	✗	Cost reduction
[19]	✗	✗	NA	✗	✗	✗	Voltage improvement
[20]	✗	✗	NA	✗	✓	✗	Cost reduction
[84]	✗	✗	NA	✗	✓	✗	Minimisation of fuel consumption
[104]	✗	✗	NA	✓	✓	✗	Operational cost reduction
[22]	✗	✗	NA	✗	✓	✗	Operational cost reduction
[25]	✗	✗	NA	✗	✓	✗	DC bus voltage regulation.
[87]	✗	✗	NA	✗	✓	✗	Fuel cost reduction
[32]	✗	✗	NA	✓	✓	✗	Operational cost reduction
[88]	✗	✗	NA	✓	✓	✗	Fuel cost reduction
[89]	✗	✗	NA	✗	✓	✗	To enhance the system power saving
[33]	✗	✗	NA	✗	✓	✗	Voltage profile improvement
[50]	A+B	✗	α	✗	✓	✗	Improvement of grid power profile
[52]	A+B	✗	$\Re$	✗	✓	✗	Cost minimisation
[60]	B	✗	$\wp$	✗	✓	✗	Voltage degradation reduction
[62]	A+B+C	✗	β	✗	✓	✗	Solution for economic dispatch problem
[64]	A+B+C	✗	$\wp$	✗	✓	✗	Cost minimisation and voltage profile improvement
[67]	A+B	✓	γ	✗	✓	✗	Probabilistic load flow solution
[68]	A+B	✓	γ	✗	✗	✗	Cost and emission reduction
[69]	A+B+C	✓	γ	✗	✗	✗	Cost and emission reduction
[70]	A+B	✓	γ	✗	✓	✓	Operational cost minimisation
[42]	✗	✗	NA	✗	✓	✓	Voltage profile improvement
[43]	✗	✗	NA	✗	✗	✓	Reliability improvement
Proposed	**A+B+C+D**	✓	γ	✓	✓	✓	**Operating cost and loss reduction**

A: Renewable sources, B: Load, C: Grid Price, D: PHEV, NA: Not applicable

α: Persistence forecasting, β: Probabilistic Numerical Method, γ: Probabilistic approximate Method, $\Re$: Receding horizon control

$\wp$: Probabilistic scenario-based approach.

- A spatiotemporal correlation exists between wind speeds at different locations within the DCμG. Further, the wind speed is also correlated with the load demand. Other input RVs are uncorrelated.

- The correlation matrix between the correlated input RVs is known.

- The hourly load demand pattern, expressed as per unit of the peak load, is the same

at all buses.

- All flexible loads shift their demand following the setpoint provided by the EMS.
- All system and network parameters (like bus connectivity, line resistances, ratings of different components, charging and discharging efficiency of BESS, etc.) are known completely.
- The study is made considering healthy system operation. i.e., the bus voltages will be maintained close to the nominal values. Therefore, a linearised network model of the DCμG can be used.

Table 2.2: Uncertainty Modelling

	Uncertainties		
	Wind	**Load/Price**	**PHEV**
Distribution	Weibull	Normal	Log-normal
pdf	Wind speed: $f_w(v_w) = \frac{x}{c}(\frac{v_w}{c})^{x-1}$ $exp[-(\frac{v_w}{c})^k]$	Load demand/Grid energy price: $PL/\pi^g \sim N(\mu_{l/g}, \sigma_{l/g})$ $f_{L/G}(PL/\pi^g) = \frac{1}{\sigma_{l/g}\sqrt{2\pi}}$ $exp\left[-\frac{((PL/\pi^g)-\mu_{l/g})^2}{2\sigma^2_{l/g}}\right]$	Daily driven distance: $f_{dist}(d) = \frac{1}{d\sigma_d\sqrt{2\pi}} exp\left[-\frac{(ln(d)-\mu_d)^2}{2\sigma_d^2}\right]$ Smart charging strategy: $f_{st}(t_{start}) = \frac{1}{3\sqrt{2\pi}} exp\left[-\frac{(t_{start}-1)^2}{18}\right]$

2.2.1 Uncertainty Modelling

The accuracy of the input data determines the correctness of a deterministic approach. Therefore, the correctness of the optimal setpoints provided by the EMS also depends on the accuracy of input variables like load demand, PHEV energy demand, generation from RES, and grid price. All the above variables are uncertain. Hence, there will always be errors in predicting the input data and consequently in the optimal setpoints provided by the EMS. Therefore, a deterministic approach is unsuitable for handling the EMS of a DCμG in the present context. It is imperative to model and incorporate the uncertainties of the input RVs in the EMS to allay the risk of the dispatch strategy [44, 45, 59, 131, 133, 138, 139, 140].

Uncertainty modelling in a power system can be done using multiple approaches like probabilistic, possibilistic, hybrid probabilistic-possibilistic, "information gap decision theory", robust optimisation, interval analysis, etc. [139, 141]. Each method has its own merits and demerits. For instance, the interval arithmetic method lacks accuracy because of expansive intervals, with increasing sources of uncertainties and system size [142, 143]. Also, interval arithmetic ignores the correlations among interval variables [144]. On the other hand, pdfs accurately model the random variability of uncertain inputs like wind speed, solar irradiance, or load demand, which follow known distributions (e.g., normal, Weibull, beta). Interval arithmetic only gives bounds, ignoring likelihood. pdfs can explicitly model correlations, which is vital for realistic analysis. Affine arithmetic partially tracks dependencies but assumes linearity and becomes complex with nonlinear or high-dimensional dependencies. Further, it gives a pessimistic estimation of the solution hull, but no quantitative mapping from input variables to output variables [144]. Also, the choice of uncertainty modelling approach depends on the nature and quantum of data available. For instance, the possibilistic technique is used when a linguistic description of the uncertain variable is available, which is amenable to representation by a fuzzy number. Severe uncertainties lacking historical data are modelled using the "information gap decision theory". Robust optimisation can be used when the uncertain variable falls within an interval. Nevertheless, it provides conservative results. The probabilistic technique is used when sufficient historical data is available to obtain a pdf for the uncertain variable. In this work, we have assumed that sufficient historical data is available for the input RVs to formulate the pdfs for modelling the uncertainties. The probabilistic method is also easy to implement [139]. Researchers have widely employed probabilistic techniques to model power system uncertainties like renewable generation, load demand, grid power price, and PHEV load profiles [141]. These techniques utilise statistical methods to assess the likelihood of different outcomes or events based on certain assumptions or data [8, 145]. We have also used a probabilistic technique to model uncertainties in this chapter.

2.2.1.1 Probabilistic modelling of input RVs

In probabilistic techniques, an appropriate pdf ($f(.)$) is used to represent an uncertain variable. In this chapter, we have used normal distribution to model load demand and

grid energy price uncertainties [8]. The wind speed uncertainty is modelled using Weibull distribution [8]. A smart charging strategy of PHEV is considered in this chapter. The charging start time is modelled using a normal distribution, while the daily travelled distance of the PHEV is modelled using a log-normal distribution [8]. The pdfs describing the input RVs are given in table 2.2.

2.2.1.2 Incorporation of correlation between input RVs

Let there be a vector $\mathbf{H} = (\wp_1, \wp_2, \ldots, \wp_m)^T$ representing m correlated RVs, where $\wp_i$ follows a pdf $f_i(.)$, and the cumulative distribution function (cdf) is $F_i(x_i)$. Let the correlation matrix be $\mathbf{R_H}$ with $\varrho_{ij}^{\wp}$ as the correlation coefficient between the RVs i and j. To generate the correlated RVs inverse NT is used since, for most of the practical applications, joint pdf of $\mathbf{H}$ is not available to generate correlated RVs. The process of using inverse NT is as follows: (1) Create a new set of standard normal vectors ($\mathbf{M}$) that are correlated with each other, starting from a set of uncorrelated standard normal vector ($\mathbf{U}$). The degree of correlation between two specific correlated standard normal variables (r_i and r_j) should be ϱ_{ij}^{m}, as indicated by the correlation matrix $\mathbf{R_M}$. (2) Generate correlated RVs ($\mathbf{H}$) from $\mathbf{R_M}$ using inverse NT. The process is given in fig. 2.1 [146]:

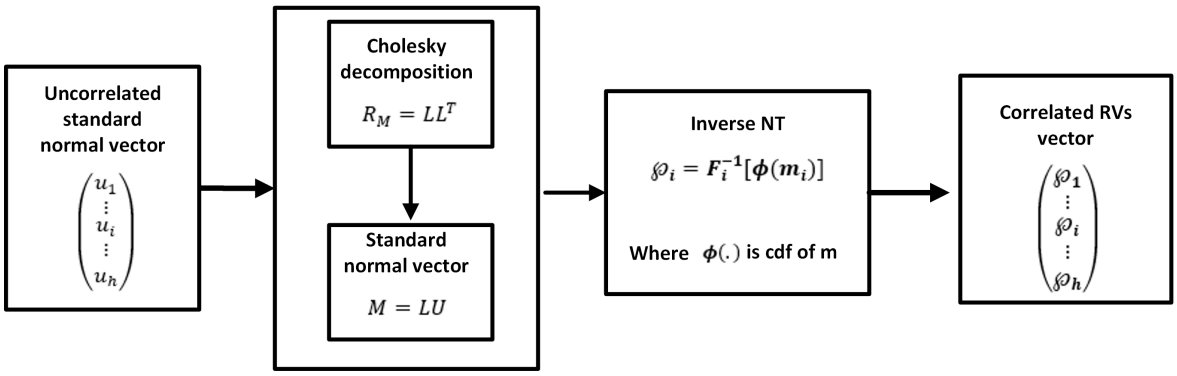

Figure 2.1: Process for incorporation of correlation

Although the correlation matrix $\mathbf{R_H}$ is known, the correlation matrix $\mathbf{R_M}$ is unavailable. As a result, $\mathbf{R_M}$ must be calculated to convert U into M. In [146], empirical formulas have been used to specify the functional relationship $\varrho_{\wp} = G(\rho_m)$ for certain marginal distributions. However, this approach does not cover a wide range of probability distributions. This chapter employs an interpolation technique to determine ϱ_M based on $\varrho_{\wp}$. The following approach is presented:

1. Choose a value for $\varrho_{ij}^{M} \in [-1, 1]$ and create the correlation matrix $\mathbf{R_M}$.

2. Obtain L by performing Cholesky decomposition on the correlation matrix $\mathbf{R_M}$.

3. Take into account y Gauss-Hermite quadrature points made up of uncorrelated standard normal vectors $\mathbf{U^i} = [u_1^i, u_2^i, \ldots, u_h^i]^T$ and $\mathbf{U^j} = [u_1^j, u_2^j, \ldots, u_h^j]^T$. Produce correlated standard normal vectors $\mathbf{M^i} = [m_1^i, m_2^i, \ldots, m_h^i]^T$ and $\mathbf{M^j} = [m_1^j, m_2^j, \ldots, m_h^j]^T$ through the transformation $\mathbf{M} = \mathbf{LU}$.

4. Create correlated vectors $\mathbf{H^i} = [\wp_1^i, \wp_2^i, \ldots, \wp_h^i]^T$ and $\mathbf{H^j} = [\wp_1^j, \wp_2^j, \ldots, \wp_h^j]^T$ by applying the inverse of NT as $\wp_l^i = F_i^{-1}[\Phi(m_l^i)]$ and $\wp_l^j = F_j^{-1}[\Phi(m_l^j)]$ $\forall l \in \{1, 2, \ldots, h\}$.

5. Calculate ϱ_{ij}^{x} using fig. 2.1 (see [146] for detail on eq. (2.1)):

$$\varrho_{ij}^{\wp} = -\frac{\mu_i \mu_j}{\sigma_i \sigma_j} + \frac{1}{\sigma_i \sigma_j}\left(\sum_{l=1}^{h}\sum_{o=1}^{h} \mathcal{L}\omega_o \wp_l^i \wp_o^j\right) \tag{2.1}$$

   $\mathcal{L}$: weight for the l^{th} Gauss-Hermite point; μ_i: Mean of the i^{th} RV; σ_i: Standard deviation of the i^{th} RV.

6. Perform steps (1) through (5) repeatedly for n values of ϱ_{ij}^{m}.

7. Utilise Newton's interpolation to construct the polynomial in eq. (2.2) with the n pairs of values $(\varrho_{ij}^{m}, \varrho_{ij}^{\wp})$ [147].

$$\varrho_{ij}^{\wp} = \sum_{l=1}^{q} \alpha_l (\varrho_{ij}^{m})^l \tag{2.2}$$

Equation (2.2) can be used to calculate the value of ϱ_{ij}^{m} for any given value of $\varrho_{ij}^{\wp}$. Once the correlation matrix $\mathbf{R_M}$ is obtained, correlated RVs ($\mathbf{H}$) is generated using fig. 2.1, and then fed to Hong's $2m$ PEM. Newton's interpolation is applied strictly within the normalised interval $[0, 1]$, using evenly spaced data points. No extrapolation beyond the known data range is performed. This controlled setup helps avoid the instability commonly associated with high-degree polynomial interpolation and ensures that the function remains well-behaved throughout the interpolation domain.

2.2.2 Hong's 2m PEM

The next step is to generate multiple evaluation points from the correlated pdfs and carry out deterministic evaluations for each of the generated evaluation points. The outputs of the deterministic evaluations are then aggregated to evaluate the moments of the output RVs. The evaluation points can be generated by MCS, analytical approaches (convolution method, cumulants technique, Taylor series expansion), or approximate methods [139]. The MCS approach is computationally burdensome since a large number of evaluation points are generated from the pdf of a RV, and deterministic evaluation is carried out for each generated evaluation point. An analytical method can reduce the computational burden but involves complicated mathematics. The approximate method provides an excellent balance between computation burden and accuracy [139]. Scenario-based modelling and PEM are two widely used approximate methods. The scenario-based modelling is uncomplicated. Nevertheless, the accuracy depends on the number of scenarios modelled. An alternative approach for generating evaluation points is to use "Hong's PEM". "Hong's PEM" is a computationally efficient approach but provides accuracy comparable to the MCS approach [139, 148]. The accuracy of a probabilistic approach is measured by taking MCS as the benchmark. Multiple investigations have revealed that the PEM method provides accuracy comparable to the MCS technique. For instance, Su has reported that the absolute error in the mean bus voltage obtained using the "Hong's 2m PEM" is no more than 0.0071% compared to the MCS simulation [148]. Another study by Jitendrantha et al. reported that the absolute percentage error in the expected generation cost obtained by using the PEM technique is $\sim 0.02 - 0.03\%$ compared to the MCS approach [69]. Hence, the PEM is highly accurate and provides reliable output for the EMS of the DCμG. The PEM technique has been widely used for uncertainty modelling in a wide range of power system applications like optimal DG and PHEV charging station placement and sizing, probabilistic power flow, available transfer capacity computation, EMS optimisation, state estimation, reliability evaluation, etc. [139, 148, 149, 150]. Since the "Hong's PEM" provides a fair trade-off between accuracy and computational burden, we have adopted the same in this work.

The uncertainties of input RVs are embedded into the computational steps and transferred to the output variables by using "Hong's 2m PEM". The evaluation points generated by the Hong's PEM are known as concentrations. Each concentration comprises

a location and a weight. The location denotes the evaluation point, while the weight is a probabilistic measure of the relative importance of the evaluation. A deterministic evaluation is carried out for each concentration. The output of each deterministic evaluation is then aggregated using the evaluation's weight to compute the output variable's moment. The size of the concentration can be defined according to the application. We have used the $2m$ method in this work, where m denotes the number of input RVs. In other words, the number of evaluation points will be twice the number of input RVs. For instance, if there are five (5) input RVs, ten (10) evaluation points are generated. Although more evaluation points can be generated by adopting $2m + 1$ or $3m$ approaches, investigations have shown the $2m$ approach to be sufficiently accurate [148].

Let $\mathbf{Z}$ denote the stochastic variable's output vector. The relation between $\mathbf{Z}$ and m input RVs $(p_1, \ldots, p_i, \ldots, p_m)$ is as follows [151]:

$$\mathbf{Z} = \mathbf{F}(p_1, \ldots, p_l, \ldots, p_m) \tag{2.3}$$

Computation steps are as follows (please see table 2.3 [151] for the mathematical expressions):

- *Step 1*: Compute the third moment of all the input RVs.
- *Step 2*: Find the coefficient of skewness for each concentration of every input RV.
- *Step 3*: Compute standard locations of all concentrations for all input RVs.
- *Step 4*: Find weights for every evaluation point.
- *Step 5*: Find the locations, i.e., the evaluation points.
- *Step 6*: Carry out deterministic evaluations for every evaluation point.
- *Step 7*: The expected output value is computed by taking the weighted sum of the outputs of deterministic evaluations.

$$E(Z_i(l,h)) = \sum_{l=1}^{m} \sum_{h=1}^{2} w_{l,h} Z_i(l,h) \tag{2.4}$$

If there are five (5) input RVs, we will compute ten (10) skewness coefficients according to the $2m$ approach. Also, we will obtain ten (10) standard locations, weights, and locations.

The number of deterministic evaluations will also be ten (10). The "Hong's PEM" method is repeated at every time step (one hour in this chapter).

Table 2.3: Hong's 2m PEM steps

Step	Computation	Equations	Description
1	Third moment for l^{th} input RV $(\forall l \in \{1, 2, \ldots, m\})$	$M_3(p_l) = \int (p_l - \mu_{pl})^3 f_{pl} dpl$	$M_3(p_l)$: third moment p_l: input RV μ_{pl}: mean of RV
2	Coefficient of skewness for h^{th} concentration $(\forall l \in \{1, 2, \ldots, m\})$	$\lambda_{l,3} = \frac{M_3(pl)}{(\sigma_{pl})^3}$	$\lambda_{l,3}$: coefficient of skewness σ_{pl}: standard deviation of RV
3	Standard location $(\forall l \in \{1, 2, \ldots, m\}, \forall h \in \{1, 2\})$	$\zeta_{l,h} = \frac{\lambda_{l,3}}{2} + (-1)^{3-h}\sqrt{m + \left(\frac{\lambda_{l,3}}{2}\right)^2}$	$\zeta_{l,h}$: standard location
4	Weights $(\forall l \in \{1, 2, \ldots, m\}, \forall h \in \{1, 2\})$	$w_{l,h} = \frac{1}{m}(-1)^h \frac{\zeta_{l,3-h}}{\zeta_l}$ Where $\zeta_l = 2\sqrt{m + \left(\frac{\lambda_{l,3}}{2}\right)^2}$	$w_{l,h}$: weight
5	Location $(\forall l \in \{1, 2, \ldots, m\}, \forall h \in \{1, 2\})$	$p_{l,h} = \mu_{pl} + \zeta_{l,h}\sigma_{pl}$	$p_{l,h}$: location
6	Deterministic evaluation for each location $(\forall l \in \{1, 2, \ldots, m\}, h = \{1, 2\})$	$\mathbf{Z}(l, h) = \mathbf{F}(\mu_{p1}, \mu_{p2}, \ldots, p_{l,h}, \ldots, \mu_{pm})$	$\mathbf{Z}$: Output vector
8	Expected value of output variable	$E(Z_i(l, h)) = \sum_{l=1}^{m} \sum_{h=1}^{2} w_{l,h} Z_i(l, h)$	E(.): Expected value

2.2.3 Modelling of DCμG components

The DCμG consists of two WPGs, four dispatchable MT units, and two BESS units. Also, a bi-directional GIC interfaces the DCμG with the upstream AC network. The GIC behaves like a slack bus. Additionally, flexible and inflexible electrical demands and PHEV loads are present. The subscript "l, h, t" denotes the h^{th} concentration for the l^{th} input RV (in Hong's PEM) at time t. The superscript b denotes the bus number. $\mathcal{B}$ and $\mathcal{T}$ denote the set of all system buses and the set of all times, respectively. A schematic diagram of the EMS is shown in fig. 2.2. The DCμGO uses the flexibility of dispatchable MT units, BESS and flexible loads to ensure load demand balance. The mentioned flexibilities can be aggregated together to form an "integrated demand response" entity to allay the risk of generation demand mismatch due to the volatility of renewable power generation [45].

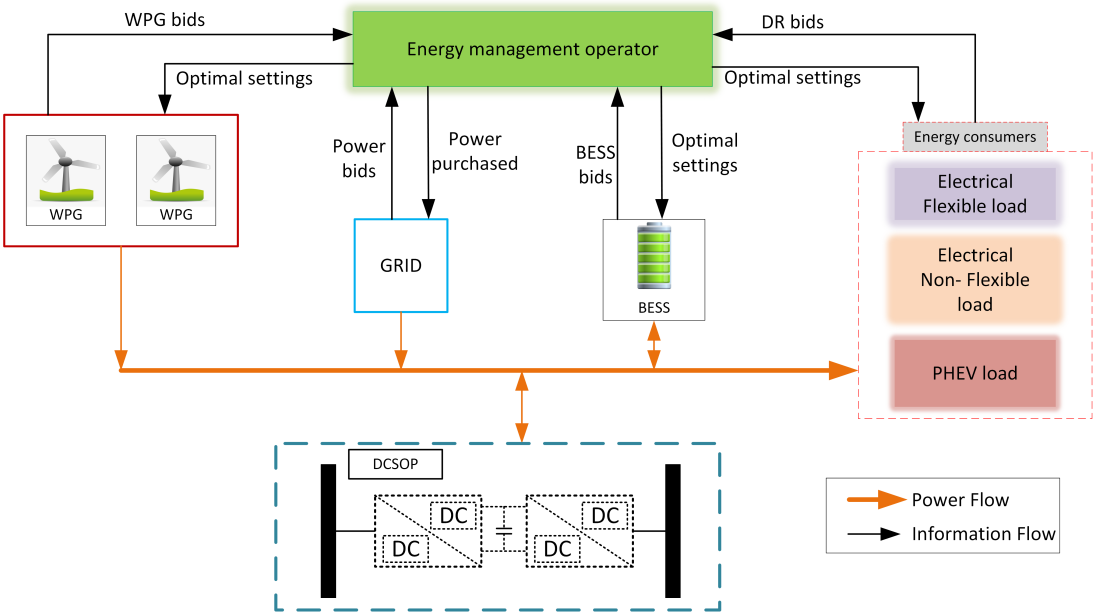

Figure 2.2: Schematic diagram of the EMS

Also, the flexible resources are optimally coordinated to achieve targeted improvements in system performance, like cost and loss minimisation. Further, the flexibility of smooth power control using DCSOP is also available to the DCμGO. The advantage of having an extensive flexibility portfolio is enhanced security and reliability of operation and improved system performance measured in terms of cost and loss minimisation.

2.2.3.1 WPG

Two WPG units are considered in this work. The available power output from the WPG is calculated using the following relations [151]:

$$PW_{l,h,t}^{avl,b} = \begin{cases} 0 & : v_{w,l,h,t}^{b} < v_{ci} \quad \& \quad v_w > v_{co} \\ a_w(v_{w,l,h,t})^3 - b_w\overline{PW} & : v_{ci} \leq v_{w,l,h,t}^{b} \geq v_{wr} \\ \overline{PW} & : Otherwise \end{cases} \tag{2.5}$$

Coefficients (a_w and b_w) follows [151]: $a_w = \frac{\overline{PW}}{(v_{wr})^3-(v_{ci})^3}$; $b_w = \frac{(v_{ci})^3}{(v_{wr})^3-(v_{ci})^3}$.

2.2.3.2 MT

A high-speed gas turbine, an MT, is also considered. A MT adjusts its active power output to meet system requirements. Consequently, MT is considered a controllable generation

source. The power output of an MT should be within the minimum and maximum generation limits, i.e.,

$$\underline{PT^b} \leq PT_t^b \leq \overline{PT^b} \tag{2.6}$$

2.2.3.3 BESS

The BESS is modelled as follows [151]:

$$EB_t^b = EB_{t-1}^b + (PBC_t^b \eta_{bc} - PBD_t^b \frac{1}{\eta_{bd}})\Delta T \tag{2.7}$$

$$0.2(\overline{EB^b}) \leq EB_t^b \leq 0.9(\overline{EB^b}) \tag{2.8}$$

$$\begin{aligned} 0 \leq PBC_t^b \leq \delta_t^{bat,c,b} \overline{PBC^b} \\ 0 \leq PBD_t^b \leq (1 - \delta_t^{bat,c,b}) \overline{PBD^b} \end{aligned} \tag{2.9}$$

$$EB_T^b = EB_0^b \tag{2.10}$$

$$\delta_t^{bat,c,b} \in \{0, 1\}; \tag{2.11}$$

ΔT: time step of optimisation. eq. (2.7) denotes charging and discharging of BESS. The DOD are DOC are limited to 80% and 90%, respectively, by eq. (2.8). The DOD and DOC constraints are imposed to avoid reduction in the BESS life expectancy due to overcharging and over-discharging. eq. (2.9) limits the charging/discharging power within the power rating of the BESS. eq. (2.10) keeps the energy the same at the beginning and end of the optimisation period. Simultaneous charging and discharging cannot occur (see eq. (2.9) and eq. (2.11)).

2.2.3.4 Flexible Load/DR Participants

The DR program allows shifting loads between periods, but there is no overall energy curtailment on a given day as given by eq. (2.12). In other words, we have considered that the DR program is activated using shiftable loads. Several devices, like washing machines,

dryers, dishwashers, water pumps, PHEV, etc., come under this category [104, 152]. The energy demands of these loads cannot be curtailed or reduced. However, the use of these devices can be shifted to periods when the electricity price is low. Therefore, a load-shifting DR program can be activated using these devices. A study in the UK has revealed that the peak energy consumption of a residential building can be shifted by $\sim 48\%$ by the use of shiftable loads [153]. The load-shifting mechanism of DR has already been reported in the literature [104, 154]. We have assumed that 10% of the total available load will participate in the DR program (given by eq. (2.13)) ($\forall l \in \{1, 2, \ldots, m\}, \forall h \in \{1, 2\}, b \in \mathcal{B}$).

$$\sum_{t\in\mathcal{T}}\sum_{l,h} w_{l,h,t} PL^{b}_{l,h,t} = \sum_{t\in\mathcal{T}}\sum_{l,h} w_{l,h,t} PL^{0,b}_{l,h,t} \tag{2.12}$$

$$0.90(PL^{0,b}_{l,h,t}) \leq PL^{b}_{l,h,t} \leq 1.10(PL^{0,b}_{l,h,t}) \tag{2.13}$$

$$\sum_{t\in\mathcal{T}}\sum_{l,h} w_{l,h,t}(PL^{0,b}_{l,h,t} - PL^{b}_{l,h,t})\pi^{DR}_{t} \geq 0 \quad : \forall b \in \mathcal{B} \tag{2.14}$$

eq. (2.14) guarantees that participants in the DR program will earn a profit from their participation.

2.2.3.5 PHEV charging load

The state of charge of a PHEV battery is determined by the all-electric range (AER) and the daily distance driven (d) [8].

$$\begin{aligned} S_{phev} &= 0 \quad : d > AER \\ &= \frac{100(AER - d)}{AER} 100\% \end{aligned} \tag{2.15}$$

The duration of charging (t_d) is as follows [8]:

$$t_{dur} = \frac{C_{bat}(1 - S_{phev})DOD}{\eta^{E}_{C} P_{chg}} \tag{2.16}$$

2.2.3.6 Network Model

The DCμG network is modelled using a symmetric G-bus matrix. The power injection at node b is given by:

$$P^{inj,b}_{l,h,t} = \sum_{n \in \mathcal{B}} G_{b,n} V^{b}_{l,h,t} V^{n}_{l,h,t} \tag{2.17}$$

(2.17) is a non-affine equality constraint, making the problem non-convex. The nodal power equation described above is linearised to obtain a convex model. The bus voltage can be expressed as follows:

$$V^{b}_{l,h,t} = 1 + \Delta V^{b}_{l,h,t}; V^{n}_{l,h,t} = 1 + \Delta V^{n}_{l,h,t} \tag{2.18}$$

Therefore, we can write (2.17) as follows:

$$P^{b}_{l,h,t} = \sum_{n \in \mathcal{B}} G_{b,n}(1 + \Delta V^{b}_{l,h,t})(1 + \Delta V^{n}_{l,h,t}) = \sum_{n \in \mathcal{B}} G_{b,n}(1 + \Delta V^{b}_{l,h,t} + \Delta V^{n}_{l,h,t} + \Delta V^{b}_{l,h,t}\Delta V^{n}_{l,h,t}) \tag{2.19}$$

The bus voltage V^b is close to the nominal value of 1 per unit under normal operating conditions, i.e., ΔV^b is small. Therefore, the term $\Delta V^{b}_{l,h,t}\Delta V^{n}_{l,h,t}$ can be neglected. Using (2.18) in (2.19) and neglecting $\Delta V^{b}_{l,h,t}\Delta V^{n}_{l,h,t}$, we can write:

$$P^{b}_{l,h,t} = \sum_{n \in \mathcal{B}} G_{b,n}(V^{b}_{l,h,t} + V^{n}_{l,h,t} - 1) = \sum_{n \in \mathcal{B}} G_{b,n} V^{b}_{l,h,t} + \sum_{n \in \mathcal{B}} G_{b,n} V^{n}_{l,h,t} - \sum_{n \in \mathcal{B}} G_{b,n} = \sum_{n \in \mathcal{B}} G_{b,n} V^{n}_{l,h,t} \tag{2.20}$$

Since G bus matrix is symmetric, $\sum_{n \in \mathcal{B}} G_{b,n} = 0$, and $\sum_{n \in \mathcal{B}} G_{b,n} V^{b}_{l,h,t} = 0$. (2.20) gives a linear model of the network.

2.2.3.7 DCSOP

We have considered two-terminal DCSOPs in this chapter. A two-terminal DCSOP comprises two back-to-back bi-directional DC-DC converters and acts as a virtual conductor. The DC-DC converters are connected to the end nodes of two feeders, as shown in fig. 2.3. Under normal operating conditions, the DCSOP operates in "$P - V_{dc}$" mode [42]. In other words, the active power reference P^* is given to one of the DC-DC converters, while the other DC-DC converter is controlled to maintain the DC-link voltage (V_{dc}). A present-day DC distribution network or DCμG comprises multiple radial feeders. The remote ends of the radial feeders often have mechanical tie switches [42]. The tie switches usually remain open to retain the radiality of the network. The tie switches are closed when a fault or

failure occurs in an upstream feeder section. Also, the network's power flow and voltage profile can be controlled by closing tie switches and opening sectionalising switches. However, such a switching scheme is called "hard switching". "Hard switching" can cause propagation of disturbances and does not allow smooth control of power flow. In contrast, a DCSOP allows soft closing with smooth power flow control in the network. DCSOPs improve the voltage profile and reduce network loss [43]. Further, the DCSOP allows supply restoration of affected feeders and reduces downtime. Therefore, system reliability improves [42]. To summarise, the main functionalities and advantages of a DCSOP are as follows [42]:

- The DCSOP enables the interconnection of multiple DC feeders with varying voltage ratings.
- During disturbances or failures, the traditional practice involves closing mechanical switches ("hard switching"). However, with a DCSOP, a more sophisticated approach, known as "soft switching", becomes possible. "Soft switching" allows smoother transitions and reduces the risk of disturbances spreading to different feeder sections.
- The DCSOP provides the capability to control and operate the feeders according to the network operator's preferences, i.e., the DCSOP can be configured to operate the feeders in radial and ring modes, offering flexibility in the network's configuration and operation.
- DCSOP ensures DC voltage regulation at the load buses, maintaining it within the desired voltage range. This regulation remains effective despite load variations, intermittent outputs from renewable sources, and varying charging profiles of PHEVs.
- The network loss can be reduced, and the system reliability can be improved using a DCSOP.

Let b and n be the end buses of two feeders. One of the DC-DC converters will be connected to bus b and the other to bus n. The steady-state equation of a DCSOP is given by the following:

$$PSOP^{b}_{l,h,t} + PSOP^{l,b}_{l,h,t} + PSOP^{n}_{l,h,t} + PSOP^{l,n}_{l,h,t} = 0 \quad \forall t \tag{2.21}$$

The apparent power ratings of the converters should not be exceeded:

$$\begin{aligned} PSOP_t^b + PSOP_t^{l,b} &\leq \overline{SSOP^b} \\ PSOP_t^n + PSOP_t^{l,n} &\leq \overline{SSOP^n} \end{aligned} \tag{2.22}$$

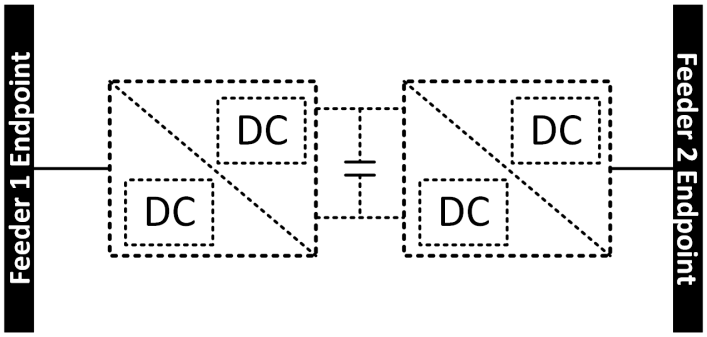

Figure 2.3: DCSOP

2.3 Problem Formulation and Solution Approach

The objectives and constraints are formulated in the probabilistic domain. The objectives are to minimise the expected values of OC and loss in a day. At every time step t, $2m$ concentrations are generated using the correlated pdfs and the "Hong's 2m PEM" approach. Deterministic analysis (i.e., finding the output variables of interest) is carried out for each concentration member. Outputs of each deterministic analysis are then aggregated by the weighted sum approach using the weights of the "Hong's 2m PEM" (see eq. (2.4)) to obtain the expected values. The process is repeated for every time step. The subscript "l, h, t" will denote the h^{th} concentration for the l^{th} input RV in the Hong's PEM at time t.

2.3.1 Objectives and Constraints

We have considered two objectives in this chapter. A MO optimisation problem can be represented as follows:

$$\begin{aligned} &\min_{\vartheta} \Psi(\chi) = [\psi_1(\chi), \psi_2(\chi)]^T \\ &s.t : \mathbf{F}(\chi) = \mathbf{0}; \mathbf{G}(\chi) \leq \mathbf{0}; \chi = [\vartheta, \kappa, \nu]^T \end{aligned} \tag{2.23}$$

Where Ψ_i: i^{th} objective; ϑ: control variables; κ: uncontrollable inputs/disturbances (renewable active power generation, non-flexible load and PHEV demand); ν: state vectors (bus voltage magnitudes). **F** and **G** denote the equality and inequality constraints, respectively.

2.3.1.1 First Objective

The first objective is to minimise the expected value of the OC (ψ_1), i.e.:

$$\min \psi_1 = \sum_t \psi_1^t \tag{2.24}$$

The expected value of the hourly OC (ψ_1^t) is computed as follows:

$$\psi_1^t = \sum_{l,h} w_{l,h,t}(C_{PG} + C_{MT} + C_{PB} + C_{DR} + C_{PW} + C_{WC} - C_{ENV}) \tag{2.25}$$

Where $w_{l,h,t}$ represents the weight corresponding to h^{th} concentration for the l^{th} RV at time t in the "Hong's PEM" method. eq. (2.25) denotes the expected value since a weighted sum of deterministic outputs is computed using "Hong's 2m PEM" concentration points and weights.

- The first term in eq. (2.25) represents the cost of active power procurement from the upstream grid. $C_{PG} = \pi_{l,h,t}^{g} P_{l,h,t}^{grid}$.
- The second term in eq. (2.25) represents the cost of procuring active power from MT: $C_{MT} = \sum_{b\in\mathcal{B}} \pi_t^{mt,b} PT_t^b$.
- The third term in eq. (2.25) is the cost of using BESS.
  $C_{PB} = \sum_{b\in\mathcal{B}} \pi_t^{bes,b}(PBD_t^b - PBC_t^b)$.
- The fourth term in eq. (2.25) is the cost of obtaining DR flexibility:
  $C_{DR} = \sum_{b\in\mathcal{B}} \pi_t^{DR,b}(PL_{l,h,t}^b - PL_{l,h,t}^{0,b})$.
- The fifth term in eq. (2.25) is the cost of procuring active power from WPGs.
  $C_{PW} = \sum_{b\in\mathcal{B}} \pi_t^{w,b} PW_{l,h,t}^b$.
- The sixth term in eq. (2.25) is the wind curtailment cost.
  $C_{WC} = \sum_{b\in\mathcal{B}} \pi_t^{wc,b} PWC_{l,h,t}^b$.

- The last term in eq. (2.25) is the environmental cost. The environmental cost will reduce when the WPG and MT are used to generate power instead of a conventional coal-based power plant. The environmental cost is $C_{ENV} = \sum_{p=1}^{3}(\sum_{b\in\mathcal{B}}((\kappa_p - ss_p)PT_t^b + \kappa_p(PW_{l,h,t}^b))(\pi_p^e + \pi_p^{pen}))$. p denotes the index of the pollutant. We have considered three polluting gases, CO_2, SO_2, and NO_x. κ_p and ss_p denote the quantity of pollutant type p emitted per unit generation from a conventional thermal unit and the MT, respectively. π_p^e and π_p^{pen} denote the environmental value and the penalty cost for the pollutant type p.

2.3.1.2 Second Objective

The second objective is to minimise the expected value of the network loss (ψ_2) in a day, i.e.:

$$\min \psi_2 = \sum_t \psi_2^t \tag{2.26}$$

The network loss is the sum of the nodal power injections. Using the linearised nodal power injection model (i.e., eq. (2.20)), we compute the expected value of the hourly network loss as follows:

$$\psi_2^t = \sum_{l,h} w_{l,h,t}(\sum_{b\in\mathcal{B}}\sum_{n\in\mathcal{B}} G_{b,n}V_{l,h,t}^n) \tag{2.27}$$

eq. (2.27) denotes the expected value since a weighted sum of deterministic outputs is computed using "Hong's 2m PEM" concentration points and weights.

2.3.1.3 Constraints

Following constraints must hold ($\forall l \in \{1,2,\ldots,m\}, \forall h \in \{1,2\}, t \in \mathcal{T}$).

- Power balance constraint ($\forall b \in \mathcal{B}$): The active power balance must always be maintained for each scenario.

$$PT_t^b + P_{l,h,t}^{grid} + PW_{l,h,t}^b - PEV_{l,h,t}^b - PBC_t^b + PBD_t^b - PL_{l,h,t}^b - PSOP_t^b = \sum_{n\in\mathcal{B}} G_{b,n}V_{l,h,t}^n \tag{2.28}$$

- Bus voltage limit constraint ($\forall b \in \mathcal{B}$): All equipment fed by the DCμG are designed to operate within a specified voltage range. Therefore, the bus voltages must lie within a specified range.

$$\underline{V} \leq V^{b}_{l,h,t} \leq \overline{V} \tag{2.29}$$

- Line current constraint ($\forall f \in \mathcal{F}$): The line current ($\mathcal{I}^{f}_{l,h,t}$) must not exceed its rated value:

$$-\overline{\mathcal{I}^{f}} \leq \mathcal{I}^{f}_{l,h,t} \leq \overline{\mathcal{I}^{f}} \tag{2.30}$$

- Grid power constraint: The rating of the GIC should not be exceeded:

$$-\overline{P^{grid}} \leq P^{grid}_{l,h,t} \leq \overline{P^{grid}} \tag{2.31}$$

- MT rating constraint: The active power generated by a MT cannot be more than the rating of the unit. eq. (2.6)

- BESS constraints: The BESS constraints have been defined by eqs. (2.7) to (2.10). Further, the following should be satisfied to ensure that the BESS does not incur loss:

$$\sum_{t \in \mathcal{T}} (PBC^{b}_{t}\eta_{bc} - PBD^{b}_{t}\frac{1}{\eta_{bd}})\Delta T \pi^{bes,b}_{t} \leq 0 \quad : \forall b \in \mathcal{B} \tag{2.32}$$

- DCSOP constraint: Power balance and power rating constraints as defined in eqs. (2.21) and (2.22)

- DR constraint: eqs. (2.12) to (2.14)

- WPG power procurement constraint: The power procured from the WPG cannot be more than the available power:

$$0 \leq PW^{b}_{l,h,t} \leq PW^{avl,b}_{l,h,t} \tag{2.33}$$

2.3.2 Solution of the MO optimisation problem

A trade-off or non-dominated solution will be determined in a MO optimisation problem. A trade-off solution will lie on the Pareto front. We have used the "epsilon-constraint" method to solve the MO optimisation problem [155]. In the "epsilon-constraint" method,

one of the objectives is considered the primary objective, while the other objectives are considered constraints. We have considered the first objective, i.e., minimisation of the OC ($\min \psi_1$), as the primary objective. The MO optimisation is formulated as:

$$\begin{aligned} &\min_{\vartheta} \psi_1(\chi) \\ &s.t : \mathbf{F}(\chi) = \mathbf{0}; \mathbf{G}(\chi) \leq \mathbf{0}; \psi_2(\chi) \leq \epsilon_2; \chi = [\vartheta, \kappa, \nu]^T \end{aligned} \tag{2.34}$$

Follow the steps given below to generate the Pareto Front:

- Optimise each objective function individually and save the results.
- Save the minimum and maximum of each objective function.
- Vary ϵ_2 in steps from minimum and maximum value and solve eq. (2.34). ψ_1 and ψ_2 will be members of the Pareto front.

Algorithm 1 Epsilon-constraint Method

Initialise index $i = 1, 2$ Define parameters $R1(i), R2(i)$

Carry out Individual optimisation

$\min_\vartheta \psi_1(\chi)$ s.t.: $\mathbf{F}(\chi) = \mathbf{0}; \mathbf{G}(\chi) \leq \mathbf{0}; \chi = [\vartheta, \kappa, \nu]^T$; $R1(1) = \psi_1$; $R2(1) = \psi_2$;

$\min_\vartheta \psi_2(\chi)$ s.t.: $\mathbf{F}(\chi) = \mathbf{0}; \mathbf{G}(\chi) \leq \mathbf{0}; \chi = [\vartheta, \kappa, \nu]^T$; $R1(2) = \psi_1$; $R2(2) = \psi_2$;

Obtain the minimum and maximum of objectives

$\psi_1^{max} = \max_i(R1(i))$,$\psi_1^{min} = \min_i(R1(i))$;

$\psi_2^{max} = \max_i(R2(i))$; $\psi_2^{min} = \min_i(R2(i))$;

Generate Pareto front

Initialise: $jo = 1$;

while $jo \leq J$ **do**

$\epsilon_2 = \psi_2^{min} + \frac{(\psi_2^{max} - \psi_2^{min})(jo-1)}{J-1}$;

Solve eq. (2.34)

Compute $\mu(\psi_i^{jo})$ using eq. (2.35) $\forall i \in \{1, 2\}$

$jo = jo + 1$;

end while

Decision making

Compute μ_D^{jo} using eq. (2.36) $\forall jo \in \{1, 2, \ldots, J\}$;

Find the best solution using eq. (2.37);

Non-dominated solutions in a Pareto front are ranked using a "fuzzy cardinal priority ranking" approach [155]. A strictly monotonic decreasing continuous membership function is assigned to the objective to be minimised. The membership function is defined as follows [155]

$$\mu(\psi_i) = \begin{cases} 1 : \psi_i \leq \psi_i^{min}; i \in \{1,2\} \\ \frac{\psi_i^{max} - \psi_i}{\psi_i^{max} - \psi_i^{min}} : \psi_i^{min} \leq \psi_i \leq \psi_i^{max}; i \in \{1,2\} \\ 0 : \psi_i \geq \psi_i^{max}; i \in \{1,2\} \end{cases} \tag{2.35}$$

Let there be J non-dominated solutions in the Pareto front. The degree of goal attainment of each non-dominated solution is measured relative to all the J non-dominated solutions as given below [155]:

$$\mu_D^{jo} = \frac{\sum_{i=1}^{2} \mu(\psi_i^{jo})}{\sum_{jo=1}^{J} \sum_{i}^{2} \mu(\psi_i^{jo})} \tag{2.36}$$

$\mu(\psi_i^{jo})$ is the membership function of the i^{th} objective of the jo^{th} non-dominated solution. A higher value of μ_D^{jo} indicates better cardinal priority ranking. Therefore, the best solution has the highest cardinal priority ranking [155]:

$$\max\{\mu_D^{jo} : jo = 1, 2, \ldots, J\} \tag{2.37}$$

2.4 Simulation studies

2.4.1 Test system

The simulation study has been carried out on a modified version of the ten-bus DCμG system reported in [156] and is shown in fig. 2.4. Line resistances are available in [156]. The system has a base voltage of 380 V and a base power of 50 kW. Other system parameters are given in table 2.4. The correlation coefficients between input RVs are shown in table 2.5 [157]. The hourly bids of different entities are given in table 2.6. The hourly wind speed and load profiles have been adopted from [151]. We have considered four classes of PHEVs as detailed in [158]. Market shares of each PHEV class were also taken from [158]. The input RVs are wind speeds experienced by the two WPGs, load demand, PHEV daily driven distance, PHEV charging process initiation time and

the energy price of the upstream grid. The two wind speeds and the load demand are considered to be correlated. Other input RVs are considered to be uncorrelated. After considering their correlations, the wind speed for the two WPG units and the load are tabulated in table 2.6. The method of obtaining PHEV charging load from the pdfs of daily driven distance and charging start time can be found in [8]. We have considered a smart charging strategy for the PHEV load. The BESS unit at bus #6 has an energy rating of 0.60 pukWh, and that connected to bus #7 has an energy rating of 1.00 pukWh. The initial SOC in both the BESS units are 60%. The GIC has a 10.0 pukW rating. Four (04) MT units are considered. Locations and sizes of the MTs are given in table 2.4. Each MT offers a bid of \$2/pukW at all hours. Further, two (02) DCSOP units are considered. Locations and sizes of the DCSOPs are given in table 2.4.

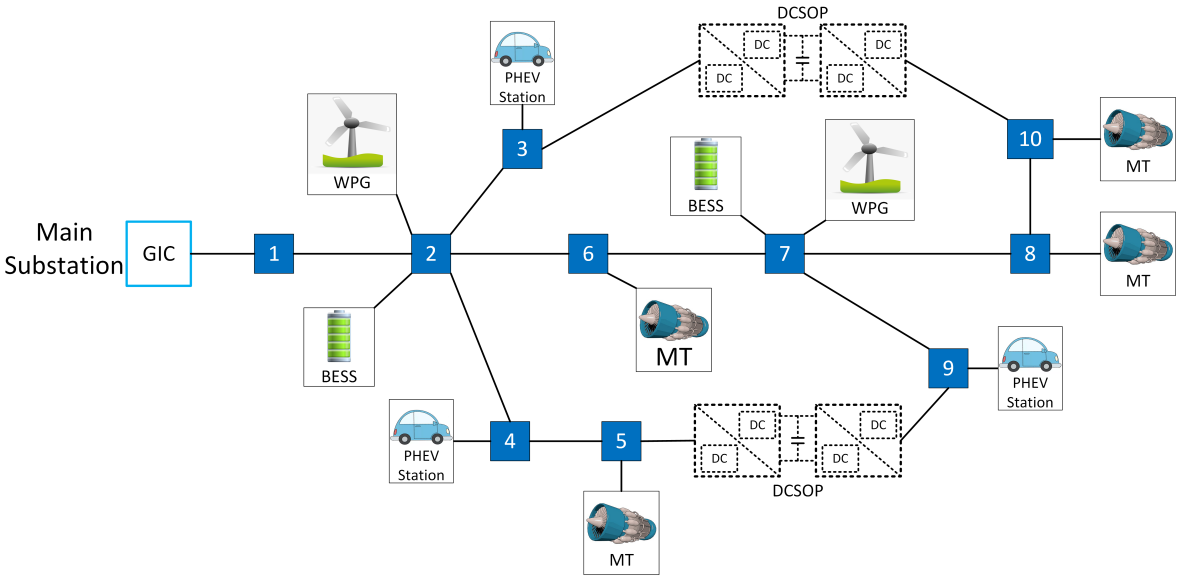

Figure 2.4: Test System

We have adopted different pollutants' environmental values and penalty coefficients for coal-based generators (representing the grid) from [159]. We have taken the environmental values of a MT as 36.77% of that of a coal-based generator. The minimum and maximum bus voltage limits are 0.95 p.u and 1.05 p.u, respectively. The codes were written on a desktop computer with Intel(R) Core(TM) i7-9700 CPU @ 3.00GHz and 16 GB RAM. The program was written using GAMS and solved by MILP with DICOPT solver version 3.17G.

Table 2.4: Test System Data

Load		**BESS**	**DG**		**SOP**
Electrical	**PHEV**		**WPG**	**MT**	
Peak load (pukW)=	Total PHEV charging station=3	Number of units=2	Number of units=2	Number of units= 4	Number of units= 2
bus 1- 0.0	Battery type= Li-ion	Bus location=2 and 7	Bus location=2 and 7	Bus location=5,6,8,10	Capacity = 2 pukW (each)
bus 2- 0.00	μ_d driven distance= 33 miles	Power rating(pukW)= 0.15 (bus-2) 0.25 (bus-7) Energy rating(pukWh)= 0.6 (bus-2) 1 (bus-7)	Capacity(pukW)= 0.30 (bus-2) and 0.50 (bus-7)	Capacity(pukW)= 3.00 (bus-5) 2.00 (bus-6) 1.30 (bus-8) 2.25 (bus-10)	Bus location between= bus- 3 and 10 bus- 5 and 9
bus 3- 1.80	σ_d driven distance= 4.517 miles	η_{bc}/η_{bd}= 95%	v_{ci}= 3 m/s		
bus 4- 2.30	Bus location= $3, 4, 9$		v_{co}= 25 m/s		
bus 5- 0.00			v_{wr}= 12 m/s		
bus 6- 0.00					
bus 7- 0.00					
bus 8- 0.00					
bus 9- 3.00					
bus 10- 0.00					

Table 2.5: Correlation between Input RVs

Uncertain Input RVs	v_{w1}	v_{w2}	PL
v_{w1}	1.00	0.87	0.21
v_{w2}	0.87	1.00	0.27
PL	0.21	0.21	1.00

2.4.2 Simulation Study and Results

The following scenarios have been considered:

- Scenario $S0$: Base case scenario.
- Scenario $S1$: The objective in this scenario is to minimise the OC (ψ_1).
- Scenario $S2$: In scenario $S2$, the EMS minimises the daily energy loss (ψ_2).
- Scenario $S3$: The MO optimisation is done in scenario $S3$.

2.4.2.1 $S0$-Base case

$S0$ is a base-case scenario. The active power is procured from the upstream grid and two WPGs. Wind power is not curtailed. No active power is procured from the MTs. DCSOP and the BESS are not scheduled. Also, the DR program is not implemented. The expected daily OC is \$247.811, while the daily expected energy loss is 1.385 pukWh. The hourly active power from the upstream grid and the WPGs are shown in fig. 2.5. The expected hourly OC and energy loss are shown in fig. 2.6a and fig. 2.6b, respectively.

Table 2.6: Hourly bids offered and mean value

Hour	**Hourly bids offered**					**Mean values after correlation**			
	π^g	π^w	π^{DR}	π^{bes}	π^{wc}	v_{w1}	v_{w2}	PL	PEV
1	1.4500	1.0000	1.2500	1.2500	0.5000	9.8937	9.8922	0.7258	0.1020
2	1.2000	1.0000	1.2500	1.2500	0.5000	9.3608	9.3590	0.6803	0.1080
3	1.1250	1.0000	1.2500	1.2500	0.5000	9.1611	9.1588	0.6299	0.1050
4	1.1500	1.0000	1.2500	1.2500	0.5000	8.9945	8.9924	0.5935	0.0930
5	1.2000	1.0000	1.2500	1.2500	0.5000	8.6946	8.6928	0.5875	0.0720
6	1.2500	1.0000	1.2500	1.2500	0.5000	8.5962	8.5916	0.5935	0.0540
7	1.4000	1.0000	1.7500	1.7500	0.5000	8.9964	8.9911	0.6057	0.0330
8	1.5500	1.0000	1.7500	1.7500	0.5000	9.0293	9.0241	0.6390	0.0210
9	1.8750	1.7500	1.7500	1.7500	0.8750	9.3279	9.3249	0.6501	0.0120
10	2.2000	1.7500	1.7500	1.7500	0.8750	9.5955	9.5907	0.7369	0.0060
11	2.1250	1.7500	1.7500	1.7500	0.8750	10.1273	10.1243	0.8005	0.0021
12	2.0000	1.7500	1.7500	1.7500	0.8750	10.2602	10.2584	0.8520	0.0009
13	2.1250	1.7500	1.7500	1.7500	0.8750	7.9625	7.9625	0.8832	0.0003
14	2.2000	1.7500	1.7500	1.7500	0.8750	7.9953	7.9951	0.8762	0.0000
15	2.3000	2.2500	2.5000	2.5000	1.1250	7.9951	7.9947	0.8590	0.0003
16	2.3500	2.2500	2.5000	2.5000	1.1250	7.7288	7.7285	0.8832	0.0006
17	2.4000	2.2500	2.5000	2.5000	1.1250	6.9638	6.9640	0.9600	0.0015
18	2.4500	2.2500	2.5000	2.5000	1.1250	5.9630	5.9627	1.0094	0.0030
19	2.5000	2.2500	2.5000	2.5000	1.1250	4.8303	4.8300	0.9902	0.0090
20	2.2500	2.2500	2.5000	2.5000	1.1250	4.4305	4.4300	0.9569	0.0150
21	1.8700	2.2500	2.5000	2.5000	1.1250	4.3307	4.3295	0.9085	0.0300
22	1.8000	2.2500	2.5000	2.5000	1.1250	4.0975	4.0972	0.8832	0.0450
23	1.5000	1.7500	1.2500	1.2500	0.8750	4.0644	4.0644	0.8086	0.0660
24	1.2500	1.7500	1.2500	1.2500	0.8750	3.9980	3.9981	0.7288	0.0870

2.4.2.2 $S1$-Cost Minimisation

The aim of the DCμGO is to procure active power from the controllable DG units,i.e., MT, WPGs and the upstream grid to minimise the OC. Further, the flexibility provided

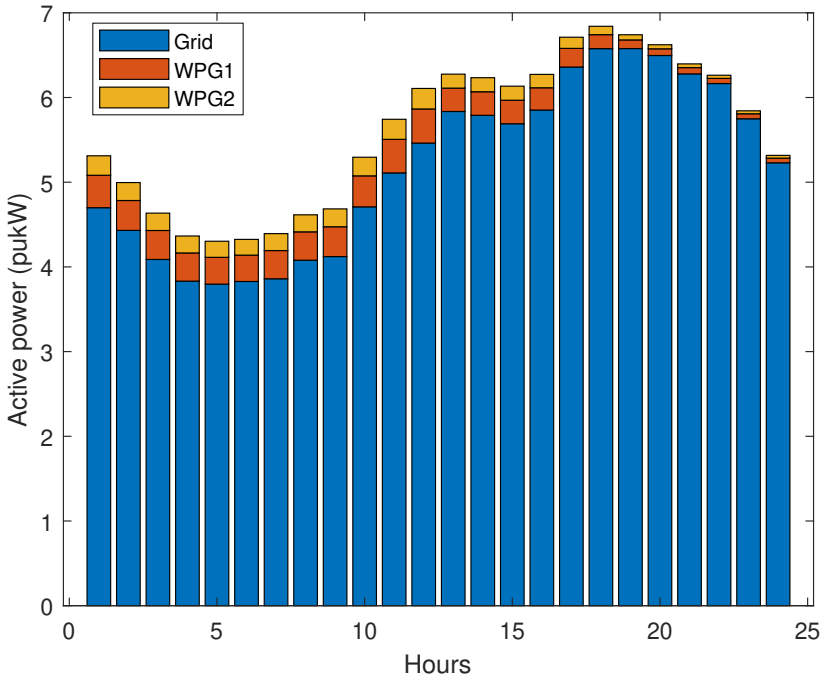

Figure 2.5: Active power procurement-$S0$ (with correlation)

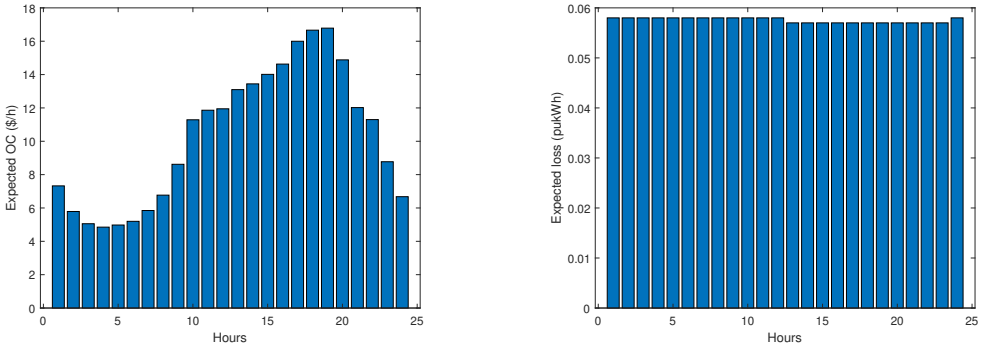

(a) Expected OC: $S0$ (b) Expected Loss: $S0$

Figure 2.6: Results for $S0$ (with correlation)

by the BESS, DR participants, and the DCSOPs are coordinated to minimise the OC. The optimal value of the OC (ψ_1) in a day is \$212.35, while the active power loss in a day (ψ_2) is 1.413pukWh. Therefore, the daily expected OC has reduced by $\sim$ 14.31% compared to scenario $S0$. On the other hand, the expected daily loss has increased by $\sim$ 2.02%. Therefore, minimising the OC enhances the system loss. The hourly expected values of OC and loss are given in table 2.7. From table 2.7, it is seen that wind power is not curtailed at any hour. In other words, all the available power from the two WPGs

are procured.

The energy contents of the two BESS are shown in fig. 2.7a. BESS unit #1 discharges during the first hour and then charges to 90% of its rated capacity considering the DOC constraint between hours #1 and #4. During hours #1 and #4, bids from all power providers are low (refer to table 2.6). Therefore, the BESS charges and stores energy during this period. The BESS discharges between hours #9 and #10, and again between hours #17 and #20. The bids of the power providers are expensive during hours #17 and #20 (refer to table 2.6). Therefore, the BESS provides arbitrage benefit. BESS #2 discharges during hours #1 and #2. During hours #3-#5, BESS#2 charges to 90% of its rated capacity considering the DOC constraint. The price of grid energy is higher during hours #1 and #2 (see table 2.6) than in hours #3-#5. Therefore, BESS#2 discharges first and then charges for providing arbitrage benefit. BESS#2 also discharges during hours #17-#19 when bids from all power providers are expensive. BESS#2 again charges during hours #23 and #24 when power prices are low.

Table 2.7: Results for scenarios -$S1$, $S2$, and $S3$ (with correlation)

	S1						**S2**						**S3**					
Hour	ψ_1	ψ_2	$PW1$	$PW2$	$PWC1$	$PWC2$	ψ_1	ψ_2	$PW1$	$PW2$	$PWC1$	$PWC2$	ψ_1	ψ_2	$PW1$	$PW2$	$PWC1$	$PWC2$
	($)	(pukWh)	(pukWh)				($)	(pukWh)	(pukWh)				($)	(pukWh)	(pukWh)			
1	7.15	0.057	0.38	0.23	0.00	0.00	8.14	0.057	0.00	0.00	0.38	0.23	7.25	0.057	0.38	0.23	0.00	0.00
2	5.76	0.057	0.35	0.21	0.00	0.00	6.50	0.057	0.00	0.01	0.35	0.21	5.77	0.057	0.35	0.21	0.00	0.00
3	4.95	0.057	0.34	0.21	0.00	0.00	5.70	0.057	0.00	0.01	0.34	0.20	4.97	0.057	0.34	0.21	0.00	0.00
4	4.77	0.057	0.33	0.20	0.00	0.00	5.51	0.057	0.00	0.00	0.33	0.20	4.78	0.057	0.33	0.20	0.00	0.00
5	4.94	0.057	0.32	0.19	0.00	0.00	5.68	0.057	0.00	0.00	0.32	0.19	4.96	0.057	0.32	0.19	0.00	0.00
6	5.19	0.057	0.31	0.19	0.00	0.00	5.91	0.057	0.00	0.00	0.31	0.19	5.20	0.057	0.31	0.19	0.00	0.00
7	5.70	0.057	0.33	0.20	0.00	0.00	6.48	0.057	0.00	0.00	0.33	0.20	5.74	0.057	0.33	0.20	0.00	0.00
8	6.68	0.057	0.34	0.20	0.00	0.00	7.51	0.057	0.00	0.01	0.34	0.19	6.71	0.057	0.34	0.20	0.00	0.00
9	8.38	0.058	0.35	0.21	0.00	0.00	9.30	0.057	0.00	0.00	0.35	0.21	8.60	0.057	0.35	0.21	0.00	0.00
10	8.28	0.062	0.37	0.22	0.00	0.00	12.07	0.057	0.00	0.00	0.37	0.22	10.64	0.057	0.37	0.22	0.00	0.00
11	9.68	0.061	0.40	0.24	0.00	0.00	12.68	0.057	0.00	0.00	0.40	0.24	11.38	0.057	0.40	0.24	0.00	0.00
12	10.90	0.061	0.40	0.24	0.00	0.00	12.75	0.057	0.00	0.00	0.40	0.24	11.71	0.057	0.40	0.24	0.00	0.00
13	11.00	0.061	0.28	0.17	0.00	0.00	13.77	0.057	0.00	0.00	0.28	0.17	12.57	0.057	0.28	0.17	0.00	0.00
14	10.48	0.061	0.28	0.17	0.00	0.00	14.12	0.057	0.00	0.00	0.28	0.17	12.55	0.057	0.28	0.17	0.00	0.00
15	10.44	0.060	0.28	0.17	0.00	0.00	14.54	0.057	0.00	0.00	0.28	0.17	12.59	0.057	0.28	0.17	0.00	0.00
16	10.79	0.061	0.26	0.16	0.00	0.00	15.20	0.057	0.00	0.00	0.26	0.16	13.09	0.057	0.26	0.16	0.00	0.00
17	12.10	0.061	0.22	0.13	0.00	0.00	16.69	0.057	0.00	0.00	0.22	0.13	13.83	0.058	0.22	0.13	0.00	0.00
18	12.89	0.061	0.17	0.10	0.00	0.00	17.73	0.057	0.00	0.00	0.17	0.10	14.59	0.058	0.17	0.10	0.00	0.00
19	12.47	0.061	0.10	0.06	0.00	0.00	17.57	0.057	0.00	0.00	0.10	0.06	14.34	0.058	0.10	0.06	0.00	0.00
20	12.23	0.060	0.08	0.05	0.00	0.00	15.56	0.057	0.00	0.00	0.08	0.05	13.84	0.057	0.08	0.05	0.00	0.00
21	11.63	0.057	0.07	0.04	0.00	0.00	12.73	0.057	0.00	0.00	0.07	0.04	11.96	0.057	0.07	0.04	0.00	0.00
22	10.69	0.058	0.06	0.04	0.00	0.00	11.68	0.057	0.00	0.00	0.06	0.04	10.95	0.057	0.06	0.04	0.00	0.00
23	8.61	0.057	0.06	0.04	0.00	0.00	9.15	0.057	0.00	0.00	0.06	0.04	8.75	0.057	0.06	0.04	0.00	0.00
24	6.66	0.057	0.06	0.03	0.00	0.00	6.97	0.057	0.00	0.00	0.06	0.03	6.69	0.057	0.04	0.03	0.00	0.01
Total	**212.35**	**1.413**	**6.13**	**3.68**	**0.00**	**0.00**	**263.92**	**1.368**	**0.00**	**0.03**	**6.13**	**3.42**	**233.43**	**1.371**	**6.12**	**3.68**	**0.00**	**0.01**

The optimal settings of the DCSOPs are shown in fig. 2.8. The feeder whose terminal bus is #3 is more heavily loaded than the feeder with terminal bus #10 during hours

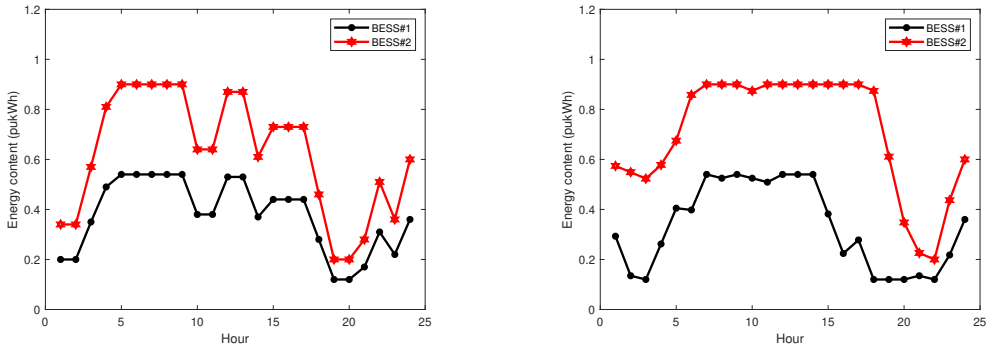

(a) Optimal BESS energy profile: $S1$ (b) Optimal BESS energy profile: $S2$

Figure 2.7: Optimal BESS profiles with correlation

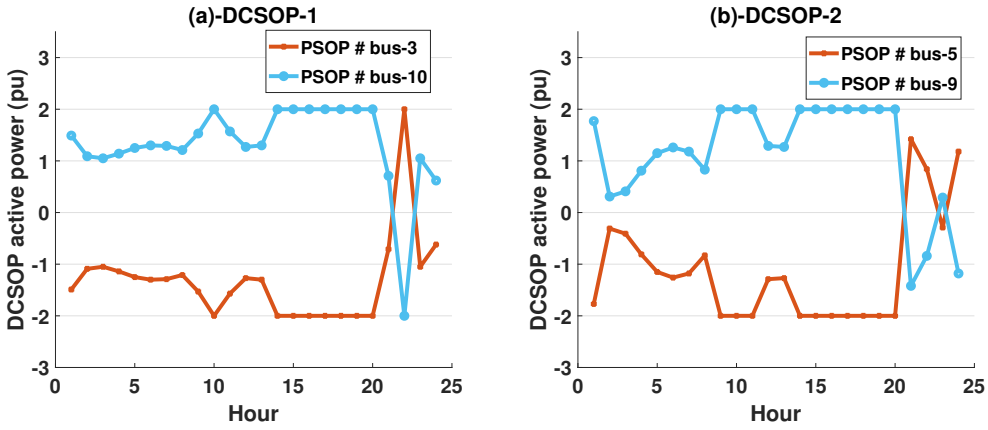

Figure 2.8: Optimised real power of DCSOP for S1 with correlation

#1-#21 and #23-#24. Therefore, the voltage source converters (VSCs) of DCSOP#1 connected to bus #10, absorbs active power from the network during hours #1-#21 and hours #23-#24. On the other hand, the VSCs of DCSOP#1, connected to bus #3, injects active power to the network during the same period. During hour #22, the VSCs of DCSOP#1, connected to bus #3, absorbs active power from the network, while at bus #3, active power is injected. A similar pattern is also observed for DCSOP#2. During hours #1 to #20 and #23, the voltage of bus #9 is higher than the voltage at bus #5. Therefore, the VSCs of DCSOP#2 absorbs active power from the network, while the VSCs of DCSOP#2, connected to bus #5 injects active power to the network during the above period. The trend reverses during hours #21, #22, and #24.

The optimal active power procurement schedule from the upstream grid and the four MTs are shown in fig. 2.9. The bid the MTs offers is \$2/pukWh at all hours. During hours #1 to #9, and #21 to #24, the price of procuring power from the upstream grid

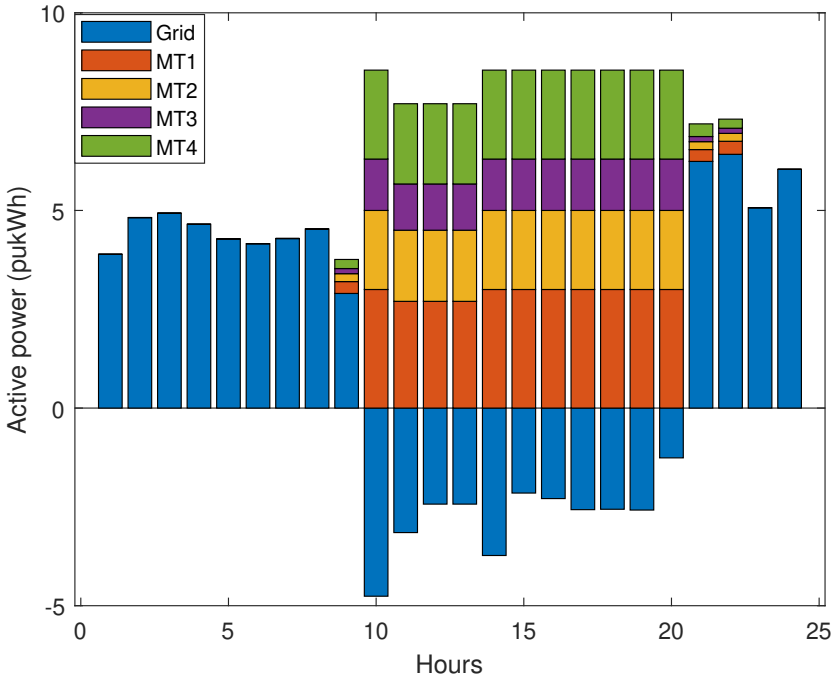

Figure 2.9: Optimised real power procurements from controllable sources- Scenario S1 (with correlation)

is lower than procuring power from the MTs (refer to table 2.6). Therefore, active power is procured mainly from the upstream grid during the period. Power procured from the MTs is relatively less. On the other hand, the grid power is more expensive than the power from the MT during hours #10-#20. Therefore, during the mentioned period, active power is procured from the MTs, and the DCμGO sells power to the upstream grid (i.e., grid power becomes negative in fig. 2.9). The load profiles before and after DR implementation are shown in fig. 2.10. The load becomes higher during hours #2 - #9,#15-#16, #20-#22, and #24 after DR implementation. On the other hand, the load demand is reduced from the original profile during other hours.

2.4.2.3 $S2$-Loss Minimisation

The objective of the DCμGO is to minimise the daily energy loss (ψ_2). The expected energy loss in a day is 1.368 pukWh, i.e., $\sim$ 1.23% lower than $S0$. On the other hand, the expected OC in a day is \$263.923, which is $\sim$ 6.50% higher than $S0$. The hourly values of OC and loss are provided in table 2.7. The results in table 2.7 show that power from the WPGs is not procured, except for hour #2, #3, and #8 for unit #2. Wind power is

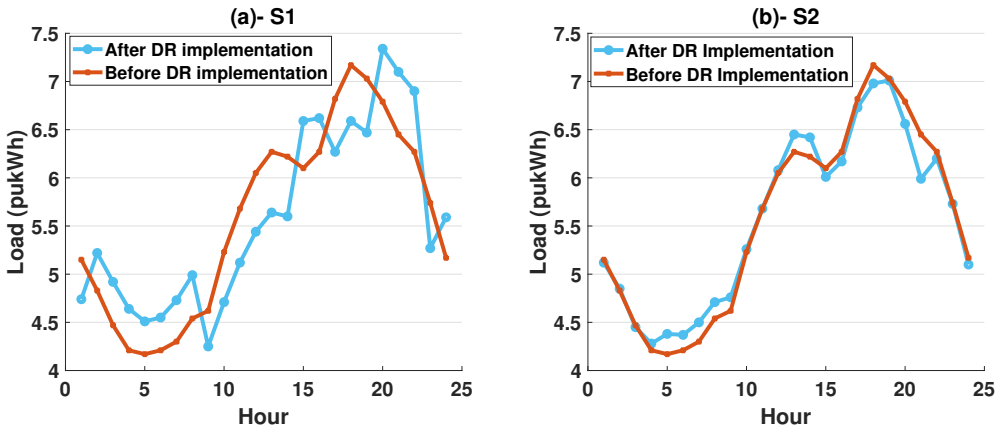

Figure 2.10: Load profiles-Before and after DR implementation (with correlation)

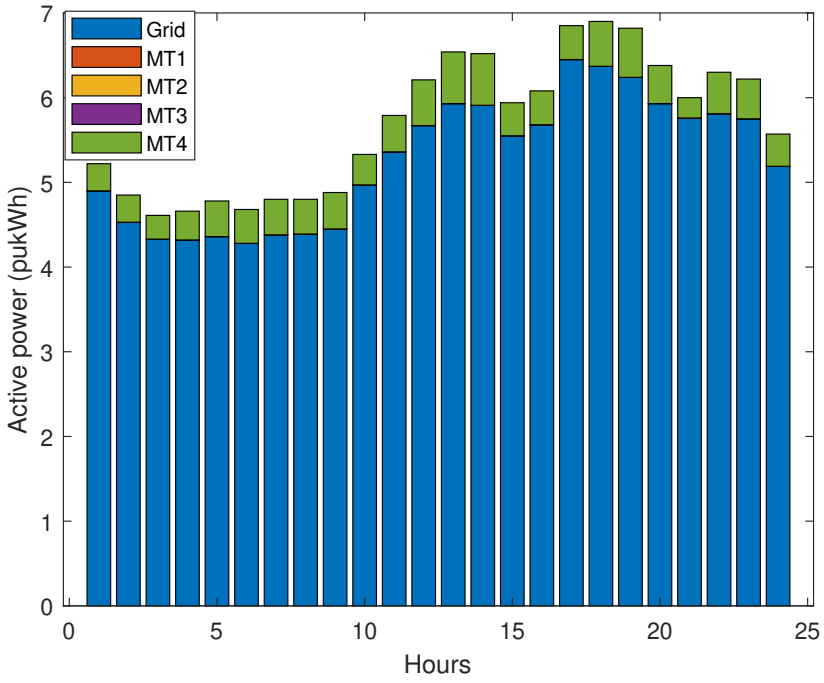

Figure 2.11: Optimised real power procurements from controllable sources- Scenario S2 (with correlation)

heavily curtailed at all hours. Optimal power procurement from the upstream grid and the MTs are shown in fig. 2.11. From fig. 2.11, we observe that power is only procured from MT#4. The upstream grid supplies the lion's share of the power. The load profile after DR implementation is shown in fig. 2.10. From fig. 2.10, we observe that a portion of the flexible load is shifted from hours #19-#22 (heavily loaded period) to hours #10-#14 (relatively lightly loaded period).

fig. 2.7b displays the energy contents of the two BESS units. From fig. 2.7b, we note

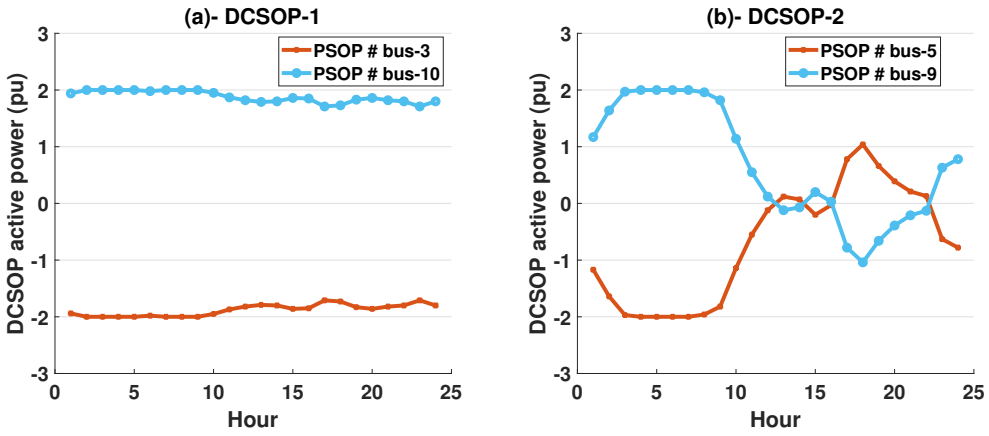

Figure 2.12: Optimised real power of DCSOP for S2 with correlation

that during hours #1 – #3, the BESS discharges. During hour #4 – #9 when the system loading is low, the BESS charges up to 90% of its rated capacity. When the system loading is high, between hours #16 – #22, BESS #1 and BESS #2 discharge. Both BESS units charge during hour #23 and hour #24. At the end of the optimisation period, the energy content of the BESS returns to its initial value.

The optimal settings of the DCSOPs are presented in fig. 2.12. From fig. 2.12, one can infer that the feeder connected to terminal bus #3 experiences higher loads throughout the day than the feeder connected to terminal bus #10. Consequently, the VSCs of DCSOP#1, linked to bus #10, absorbs active power from the network. Conversely, the VSCs of DCSOP#1, connected to bus #3, injects active power at bus #3. DCSOP#2 is connected between buses #5 and #9. During hours #1 to #12, #15, #16, #23, and #24, bus #9 has a higher voltage than bus #5. Therefore, the VSCs of DCSOP#2, connected to bus #9, absorbs active power from the network. Conversely, during the same period, the VSCs of DCSOP#2, connected to bus #5, injects active power into the network. However, this trend reverses during hours #13, #14 and #17 – #22.

2.4.2.4 $S3$-MO optimisation

From scenarios $S1$ and $S2$, we observe that minimisation of OC increases the loss and vice versa. Therefore, a trade-off solution is needed to simultaneously minimise the OC and loss. We have used the "epsilon-constraint" method to solve the MO optimisation problem. The Pareto front is shown in fig. 2.13. The Pareto front comprises several non-dominated solutions. All non-dominated solutions are assigned cardinal priority rankings

using the method described in section 2.3.2. The non-dominated solution having the highest cardinal priority ranking is also marked in fig. 2.13.

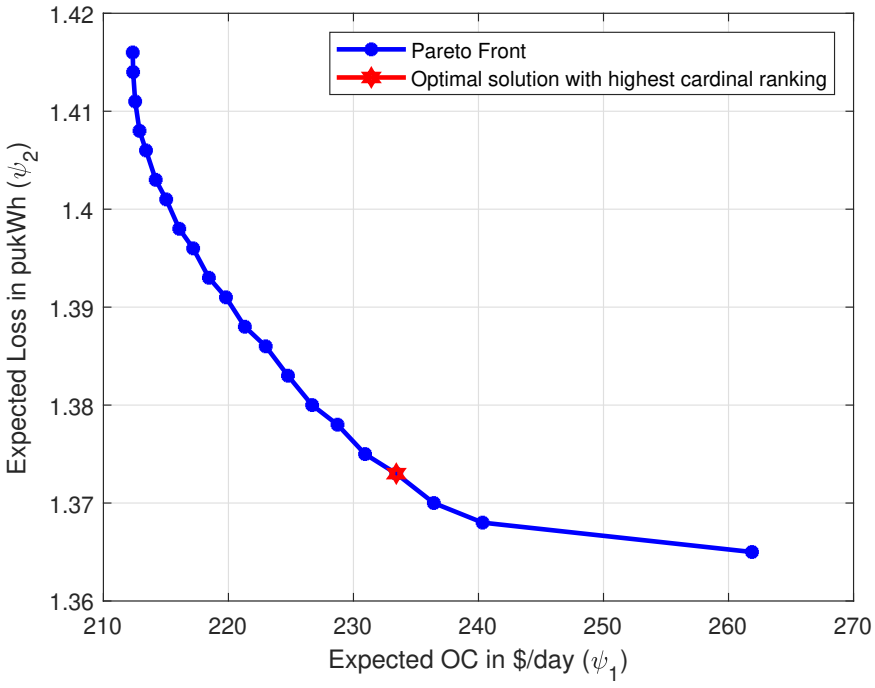

Figure 2.13: Pareto Front- $S3$ (with correlation)

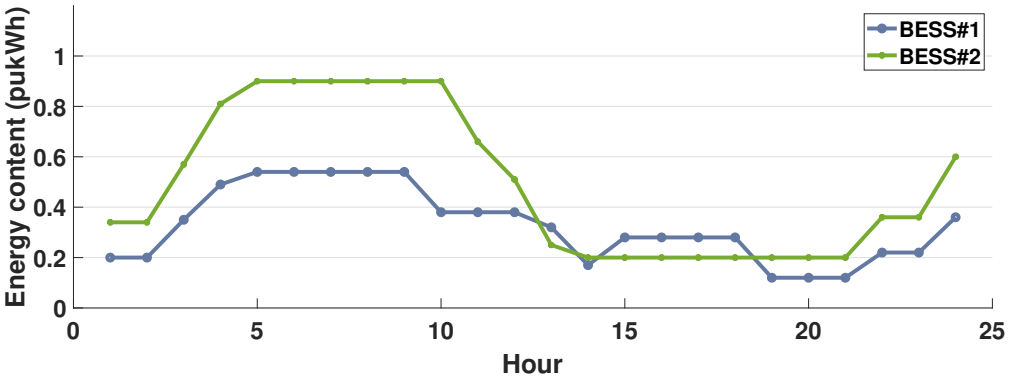

Figure 2.14: Optimal BESS profiles for S3 with correlation

The results for the optimal solution having the highest cardinal priority ranking are summarised in table 2.7. The expected OC in a day is \$233.43, which is $\sim 5.80\%$ lower than $S0$. On the other hand, the expected energy loss in a day is 1.371 pukWh, which is $\sim 1.01\%$ lower than $S0$. Further, we note that wind power is not curtailed at any hour except hour#24 for WPG#2. In other words, almost all the available power from the two WPGs are procured.

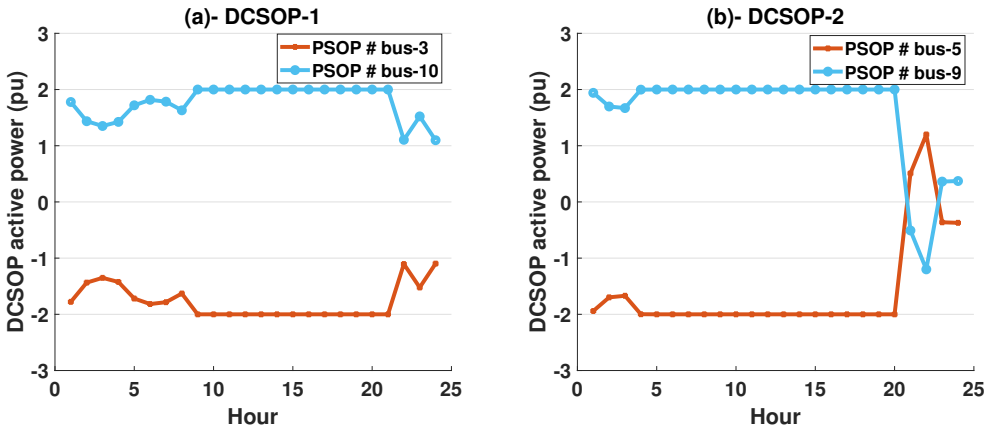

Figure 2.15: Optimised real power of DCSOP for S3 with correlation

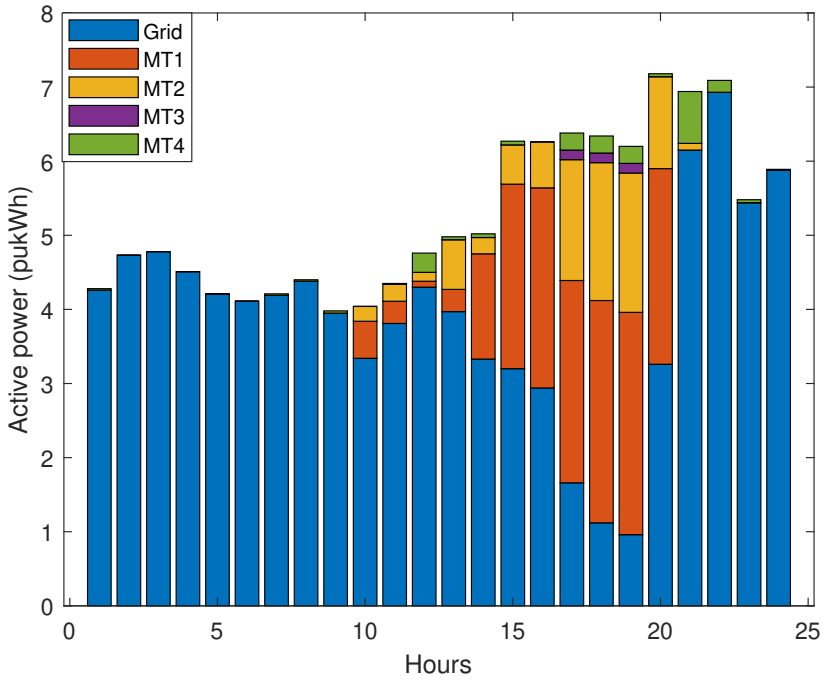

Figure 2.16: Optimised real power procurements from controllable sources- Scenario S3 (with correlation)

In fig. 2.14, the energy levels of two BESS units are displayed. Both units discharged from hour #1 to hour #3. From hour #4 to hour #9, both units charged up to their rated values. Similarly, both units discharged again from hour #10 to hour #21 due to the higher load.

The optimal settings of the DCSOPs are presented in fig. 2.15. From fig. 2.15, it can be deduced that the feeder linked to terminal bus #3 undergoes higher loads throughout the day than the feeder connected to terminal bus #10. As a result, the

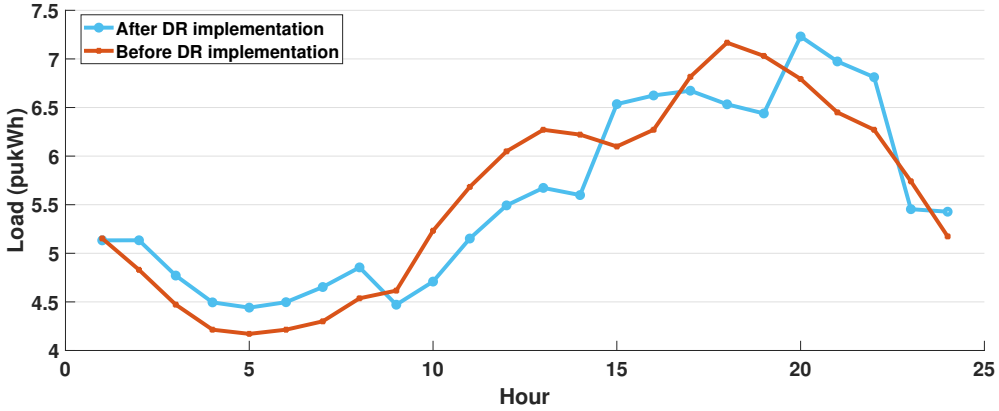

Figure 2.17: Load profiles-Before and after DR implementation for S3 with correlation

VSCs of DCSOP#1 that is connected to bus #3, injects active power into bus #3, while the VSCs of DCSOP#1 that is linked to bus #10 absorbs active power from the network. The DCSOP#2 is installed between buses #5 and #9. The voltage at bus #9 is higher than the voltage at bus #5 during hours #1 to #20 and #23 – #24. Hence, the VSCs of DCSOP#2, connected to bus #9, absorbs active power from the network. However, during the same period, the VSCs of DCSOP#2, connected to bus #5, injects active power into the network. Nevertheless, this trend reverses during hours #21 and #22.

The procurement schedule for optimal active power from both the upstream grid and the four MTs is presented in fig. 2.16, with the MTs offering a bid of \$2/pukWh consistently across all hours. The load profiles before and after the implementation of DR are illustrated in fig. 2.17. Throughout hours #1 to #9, and #21 to #24, a bulk amount of power is procured from the upstream grid, MTs supply a relatively small quantity of active power. As a result, active power is primarily obtained from the upstream grid during this period, with power from the MTs being used to a lesser extent. Conversely, during hours #10-#20, grid power is more expensive than MT power. Therefore, active power is also sourced from the MTs during this specified timeframe.

2.4.2.5 Impacts of different flexibilities on system performance

The impacts of different flexibilities on the objectives are given in table 2.8.

- *Scenario S*1: When the DR is not considered the loss increases by $\sim$ 0.14% and the OC increases by $\sim$ 1.46%. The impact of DCSOP on the OC is negligible. However, the loss increases by $\sim$ 1.56% when DCSOP is not used. The impact of

BESS on loss is negligible, but OC increases by $\sim 0.41\%$ if BESS is not considered. The impact of MT is on both OC (increases by $\sim 16.56\%$ without MT) and loss (decreases by $\sim 2.47\%$ without MT). The impact of WPG on loss is negligible, but OC increases by $\sim 5.41\%$ in the absence of WPGs.

- *Scenario* $S2$: The effect of DR on loss is insignificant. However, the OC increases by $\sim 0.73\%$ if DR is not implemented. Without DCSOP the OC decreases by $\sim 0.16\%$. On the other hand, DCSOP reduces the network loss. The loss increases by $\sim 0.87\%$ if DCSOP is not considered. The impact of BESS, WPG, and MTs on loss are insignificant in scenario $S2$. BESS affects OC (increases by $\sim 0.05\%$ without BESSs). MT affects OC (decreases by $\sim 0.78\%$ without MTs). The impact of WPG on OC is negligible.

- *Scenario* $S3$: The impacts of DR on OC and loss are insignificant. DCSOP affects both OC and loss in scenario $S3$. The OC decreases by $\sim 1.22\%$ while the loss increases by $\sim 2.04\%$ without DCSOPs. The impact of BESS and MT on loss is small. However, the OC decreases by $\sim 0.80\%$ when the flexibility of BESS is not considered. On the other hand, the OC increases by $\sim 6.30\%$ if power is not procured from the MTs. The WPGs affect both the OC and the loss. The OC increases by $\sim 1.49\%$, and the loss increases by $\sim 0.65\%$ if power is not procured from the WPGs.

The best system performance is obtained considering all the flexibilities available to the DCμGO.

Table 2.8: Impact of different flexibilities with correlation

Scenario	Performance Index	With all flexibilities	Without DR	Without SOP	Without BESS	Without MT	Without WPG
S1	**OC ($/day)**	212.35	215.452	212.450	213.215	247.518	223.852
	Loss (pukWh)	1.413	1.415	1.435	1.416	1.378	1.414
S2	**OC ($/day)**	263.92	261.974	263.499	264.067	261.859	263.505
	Loss (pukWh)	1.368	1.366	1.380	1.365	1.366	1.365
S3	**OC ($/day)**	233.43	233.485	230.58	231.542	248.143	236.921
	Loss (pukWh)	1.371	1.375	1.399	1.375	1.370	1.380

Table 2.9: Comparison of results with uncorrelated RVs

Performance Index	Scenario# S1		Scenario# S2		Scenario# S3	
	With Correlation	Without Correlation	With Correlation	Without Correlation	With Correlation	Without Correlation
Daily OC ($/day)	212.35	210.16	263.92	261.78	233.43	228.66
Daily Loss (pukWh)	1.413	1.417	1.368	1.368	1.371	1.376
WPG-1 power in a day(pukWh)	6.13	6.13	0	0	6.12	6.13
WPG-2 power in a day(pukWh)	3.68	3.68	0.03	0.11	3.68	3.68
Grid power in a day(pukWh)	32.31	31.12	126.50	124.54	95.40	88.84
MT1 power in a day(pukWh)	33.03	33.03	0.00	0	19.17	20.95
MT2 power in a day(pukWh)	22.00	22.00	0.00	0.03	9.29	11.79
MT3 power in a day(pukWh)	14.30	14.30	0.00	0.00	0.39	0.78
MT4 power in a day(pukWh)	24.85	24.78	10.22	10.80	2.13	2.80

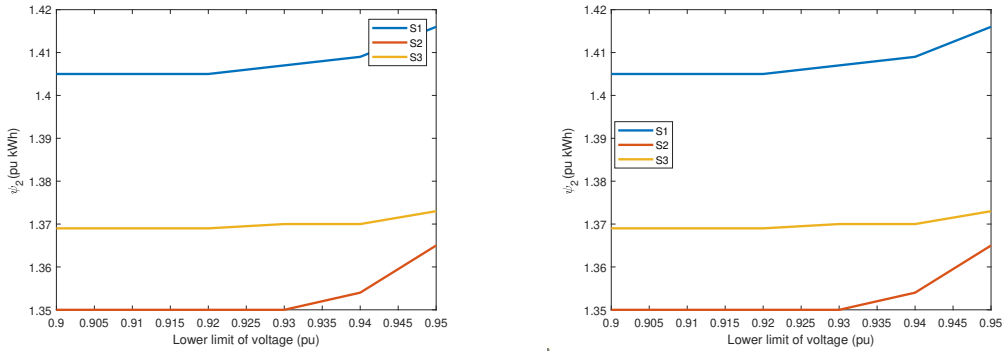

(a) Expected OC with lower voltage limit (b) Expected Loss with lower voltage limit

Figure 2.18: Sensitivity of lower voltage limit

2.4.2.6 Sensitivity analysis

1. *Impact of voltage lower limit constraint:* The lower bound of the bus voltage is varied between 0.90 pu to 0.95 pu, and the impact on the expected OC and loss are plotted in fig. 2.18a and fig. 2.18b, respectively.

   - *Impact on OC (see fig. 2.18a):* In scenario $S1$, the expected OC is insensitive to the lower voltage limit. In other words, in scenario $S1$, the optimal values of the bus voltages are more than 0.95 pu. Therefore, a reduction in the lower

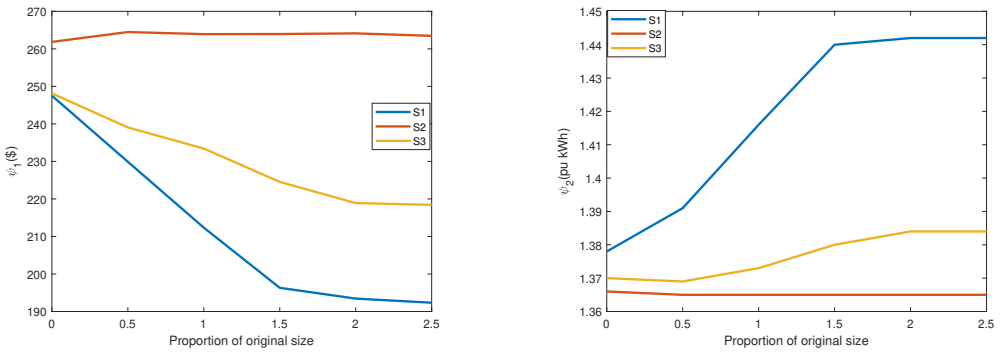

(a) Expected OC with MT rating (b) Expected Loss with MT rating

Figure 2.19: Sensitivity of MT rating

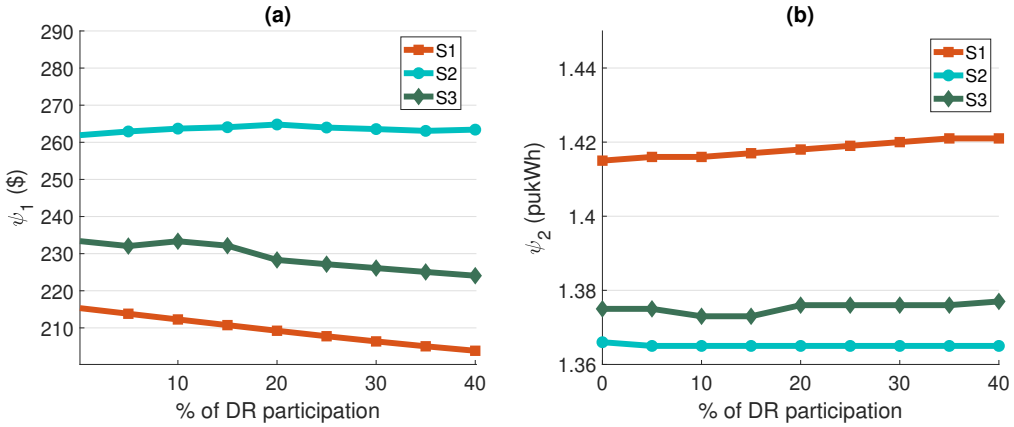

Figure 2.20: Sensitivity of DR participation

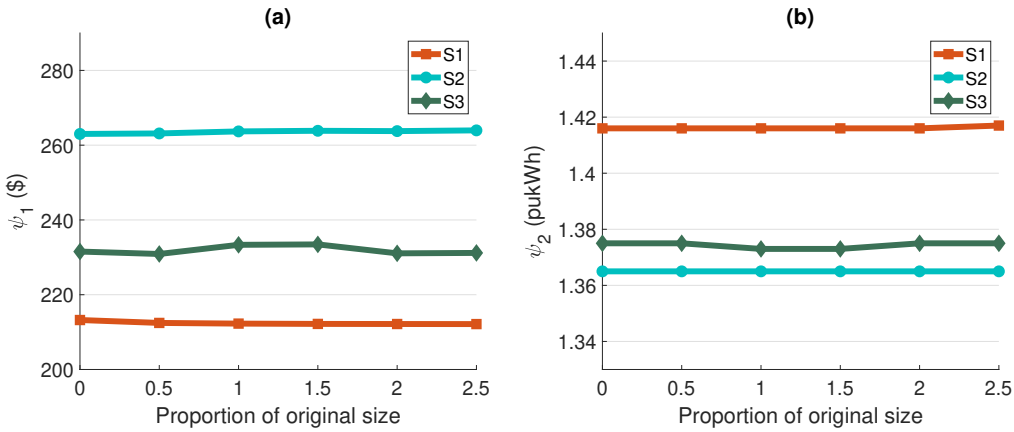

Figure 2.21: Sensitivity of BESS size

limit does not impact the expected OC. In scenarios $S2$, the OC remains almost constant ($\sim$ \$263.183) when the lower bound of the bus voltage is within 0.90 pu and 0.94 pu. The OC increases slightly to $\sim$ \$263.923 beyond 0.94 pu.

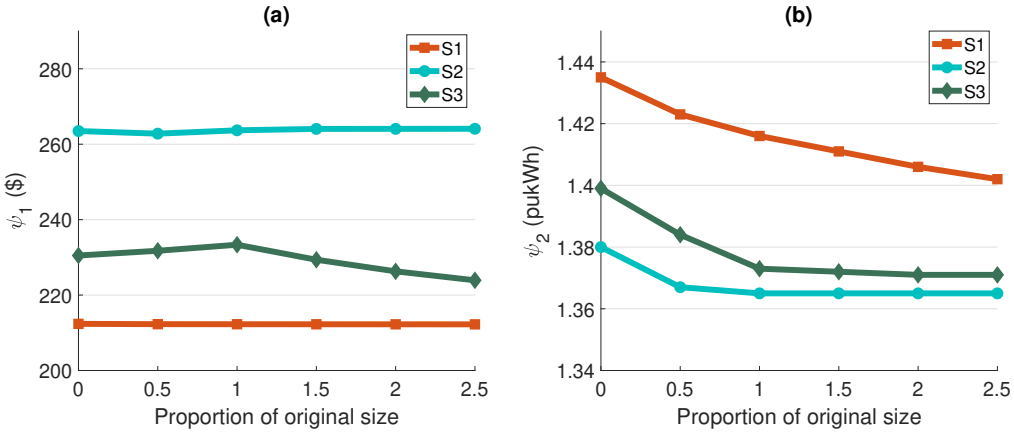

Figure 2.22: Sensitivity of DCSOP size

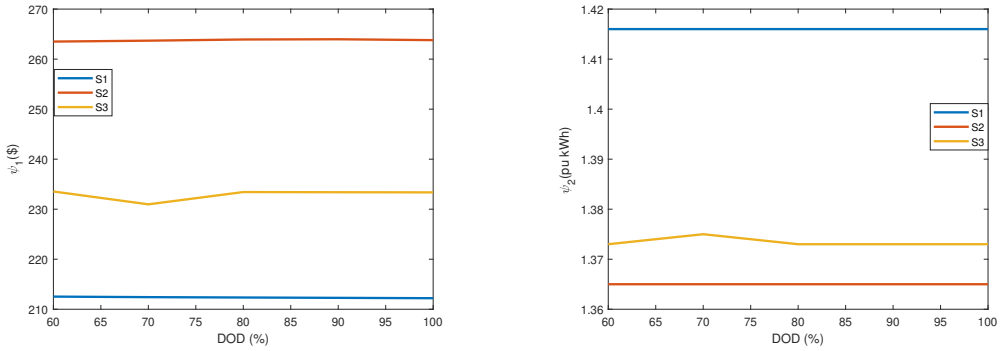

(a) Expected OC with DOD (b) Expected Loss with DOD

Figure 2.23: Sensitivity of DOD of the BESS

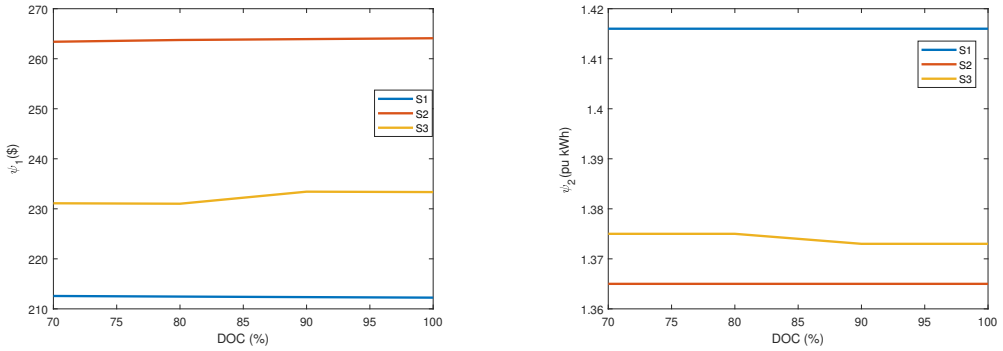

(a) Expected OC with DOC (b) Expected Loss with DOC

Figure 2.24: Sensitivity of DOC of the BESS

In scenarios $S3$, the OC remains substantially the same ($\sim$ \$230.175) with the lower limit of bus voltage varying between 0.90 pu and 0.93 pu. The OC increases to $\sim$ \$230.41 when the lower limit of the bus voltage is set to 0.95

pu.

- *Impact on loss (see fig. 2.18b):* In scenario, $S1$, the loss remains almost the same ($\sim$ 1.405 pukWh) with the bus voltage lower bound varying between 0.90 pu and 0.92 pu. The loss increases to $\sim$ 1.416 pukWh when the bus voltage lower bound is 0.95 pu. For scenarios $S2$ and $S3$, the loss is insensitive with the bus voltage lower bound varying between 0.90 pu to 0.93 pu. The loss increases as a more stringent lower bound is imposed on the voltage.

2. *Impact of MT rating constraint:* The impacts of MT size on the OC and loss are investigated.

   - *Impact on OC (see fig. 2.19a):* In scenario $S1$, the OC reduces from $\sim$ \$247.518 to $\sim$ \$192.342 as the size of all the MTs vary from 0% to 250% of the nominal ratings. The OC is more sensitive to the MT rating up to 150% of the nominal rating considered in this study. The economic benefit of increasing the MT size is comparatively lower beyond 150% of the nominal rating. In scenario $S2$, the objective is to minimise the loss. Therefore, the OC increases when the MT size is increased from 0% to 50% of the nominal rating because the flexibility of the MT reduces the loss slightly, which is the objective. Above 50% of the nominal rating, the OC becomes insensitive to MT size. In scenario $S3$, the OC reduces from $\sim$ \$248.143 to $\sim$ \$218.427 as the MT sizes are varied from 0% to 250% of the nominal ratings. However, the economic benefit reduces once the MT size touches 200 % of the nominal rating.

   - *Impact on loss (see fig. 2.19b):* In scenario $S1$, the loss increases from $\sim$ 1.378 pu kWh to $\sim$ 1.442 pukWh as the rating of the MTs are increased from 0% to 250% of the nominal rating because the flexibility of the MT is used to reduce the cost resulting in a consequent increase in the loss. The sensitivity is low for MT ratings higher than 150% of the nominal rating. In scenario S2, the loss reduces slightly from $\sim$ 1.366 pukWh to $\sim$ 1.365 pukWh as the rating varies from 0% to 250%. In scenario S3, the loss increases from 1.37 pukWh to 1.384 kWh with MT size varying from 0% to 250% of the nominal ratings.

3. *Impact of DR participation constraint:* The % of DR participation is varied in steps between 0% to 40%, and the impacts on OC and loss are plotted in fig. 2.20.

- *Impact on OC:* For scenario $S1$ and $S3$, OC decreases as the DR participation increases from 0% (OC is $\sim$ \$215.36 for $S1$ and $\sim$ \$233.41 for $S3$) to 40% (OC is $\sim$ \$203.84 for $S1$ and $\sim$ \$224.06 for $S3$). For scenario $S2$ OC first increases from 0% ($\sim$ \$261.90) to 20% ($\sim$ \$264.79) of DR participation and then decreases from 25% ($\sim$ \$263.98) to 40% ($\sim$ \$263.41) of DR participation (given in fig. 2.20).
- *Impact on loss:* For scenario $S1$ loss increases as the DR participation increases from 0% (loss is $\sim$ 1.415 pukWh for $S1$ and $\sim$ 1.375 pukWh for $S3$) to 40% (loss is $\sim$ 1.421 pukWh for $S1$ and $\sim$ 1.377 pukWh for $S3$). For scenario $S3$, loss first decreases from 0% (1.375 pukWh) to 15% (1.373 pukWh) of DR participation. For the scenario, $S2$ loss remains the same (given in fig. 2.20).

4. *Impact of BESS size constraint:*
   - *Impact on OC:* The OC reduces slightly with increasing BESS rating for scenario $S1$ (see fig. 2.21). For scenario $S2$, the OC is not sensitive to the BESS rating. However, for scenario S3, the OC increases when the BESS size varies 1 (OC is $\sim$ \$233.346) to 1.5 (OC is $\sim$ \$1.373) times the original size.
   - *Impact on loss:* The loss remains nearly unchanged despite variations in the proportion of BESS size, as outlined in fig. 2.21. However, for scenario S3, the loss decreases ($\sim$ 1.373 pukWh) when the BESS size varies 1 to 1.5 times the original size.
5. *Impact of DCSOPs size constraint:*
   - *Impact on OC:* For scenarios $S1$ and $S2$, the OC remains nearly unchanged despite variations in the proportion of DCSOP size, as outlined in fig. 2.22. However, for $S3$ OC decreases when DCSOP size is increased from 1.5 (OC is $\sim$ \$229.37) to 2.5 (OC is $\sim$ \$223.92) times the original size.
   - *Impact on loss:* The loss decreases when the DCSOP size is increased for all scenarios as given in fig. 2.22.
6. *Impact of BESS DOD constraint:* The DOD of both the BESS units are varied from 100% (i.e., fully allowed to discharge) to 60% (i.e., minimum SOC should be 0.4), and the impact is studied.

- *Impact on OC (see fig. 2.23a):* For the system under consideration, the DOD of the BESS has a negligible effect on the expected OC.
- *Impact on loss (see fig. 2.23b):* Likewise, the DOD of the BESS in the considered range has an insignificant impact on the expected loss of the system over a day.

7. *Impact of BESS DOC constraint:* The DOC of both the BESS units are varied from 70% (i.e., allowed to charge up to 70% of the capacity) to 100% (i.e., allowed to charge fully up to energy rating), and the impact is studied.

   - *Impact on OC (see fig. 2.24a):* For the system under consideration, the DOC of the BESS has a negligible effect on the expected OC.
   - *Impact on loss (see fig. 2.24b):* Likewise, the DOC of the BESS in the considered range has an insignificant impact on the expected loss of the system over a day.

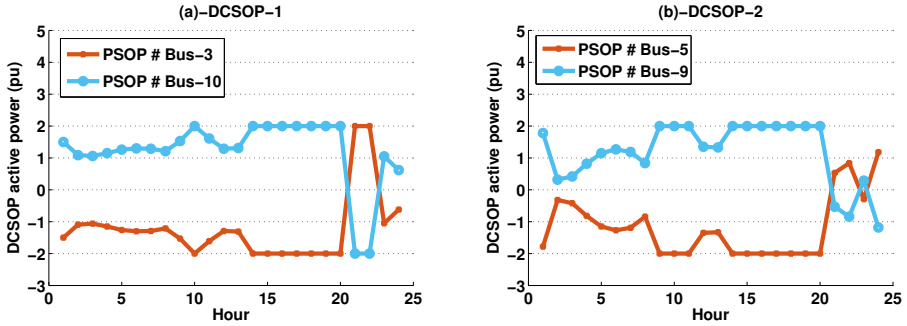

Figure 2.25: Optimised real power of DCSOP for S1 without correlation

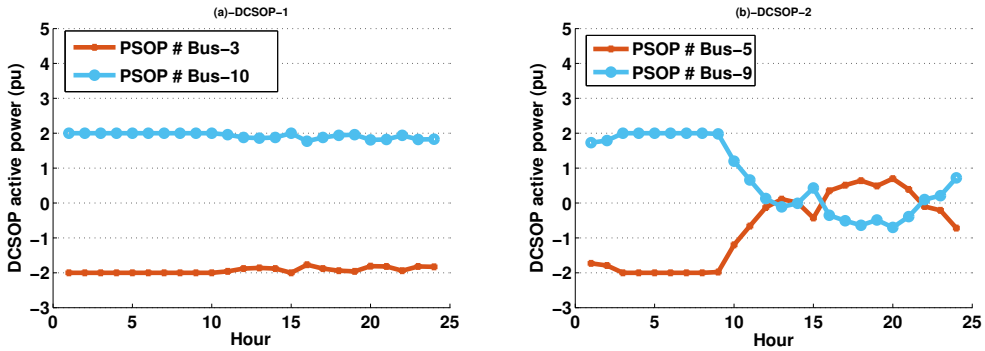

Figure 2.26: Optimised real power of DCSOP for S2 without correlation

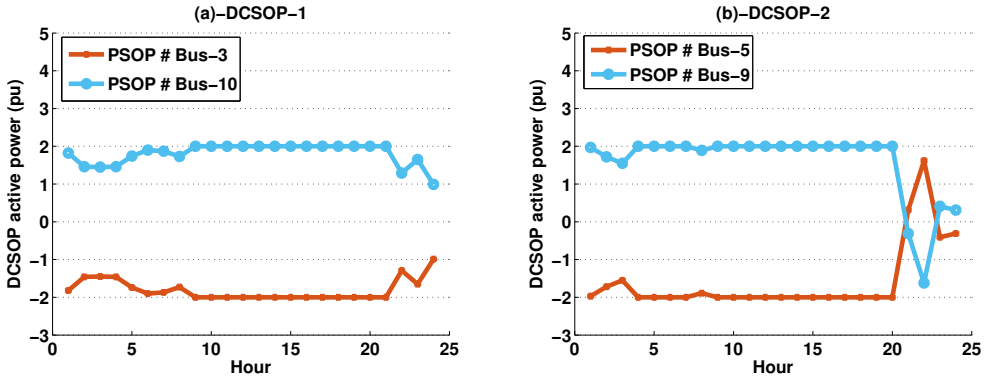

Figure 2.27: Optimised real power of DCSOP for S3 without correlation

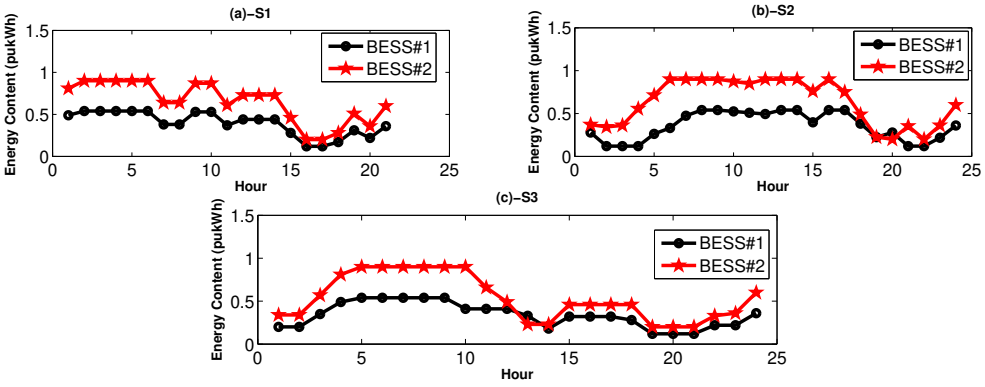

Figure 2.28: Optimal BESS profiles without correlation

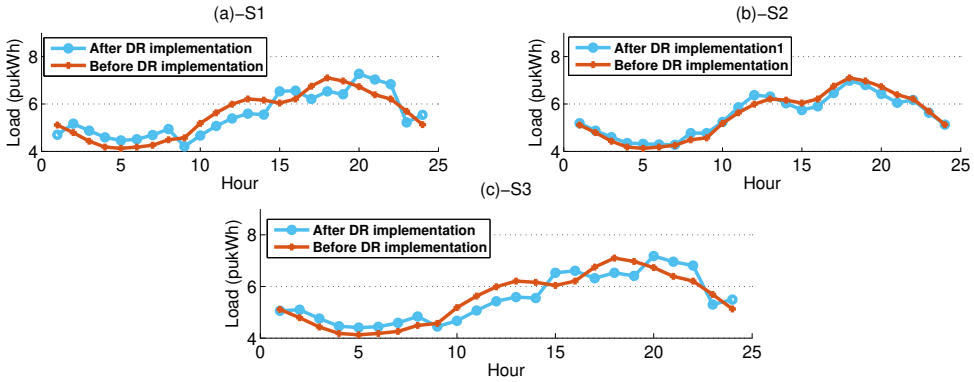

Figure 2.29: Load profiles-Before and after DR implementation (without correlation)

2.4.2.7 Performance comparison with correlated and uncorrelated input RVs

A comparison of system performance and the optimal settings of different flexibilities with and without correlation between the input RVs is summarised in table 2.9.

- *Scenario S1*: The OC is $\sim 1.03\%$ higher if the correlation between the input RVs is considered. However, the loss is $\sim 0.28\%$ lower when the correlation is considered.

Further, the DCμGO procures $\sim 3.82\%$ more energy from the upstream grid with correlated input uncertainties. There is no impact of correlation on the energy procurement schedules from the two WPG units and MTs $\#1 - \#3$. On the other hand, $\sim 0.28\%$ more energy is procured from MT #4 with correlated input RVs. The optimal setpoints of the DCSOPs are shown in fig. 2.25. Optimal setpoint values of both DCSOP units vary slightly with and without correlation between the input RVs. However, the trends are similar with and without correlation between the uncertain variables.

- *Scenario S2*: The expected daily loss remains almost the same, while the OC is $\sim 0.81\%$ higher when the correlation between the input RVs is considered. The DCμGO procures $\sim 1.57\%$ more energy in a day from the upstream grid when correlated input RVs are taken. On the other hand, the daily energy procurement from MT #4 reduces by $\sim 5.37\%$ with correlated input RVs. A negligible amount of energy is procured from the WPG units and the other three MTs. The optimal settings of the DCSOPs are shown in fig. 2.26. The impact of correlation on the optimal setting of DCSOP #1 is negligible. On the other hand, the impact of correlation is more pronounced on the optimal setpoint of DCSOP #2.

- *Scenario S3*: In the MO optimisation case, the loss is $\sim 0.36\%$ lower while the OC is $\sim 2.04\%$ higher when the correlation is considered. The power procurement schedules from the two WPG units are almost identical with and without correlation between the input RVs. The DCμGO procures $\sim 7.38\%$ more energy from the upstream grid with correlated input RVs. On the other hand, the DCμGO reduces energy procurement from the four MTs with correlated RVs. Energy procurement from MT #1 reduces by $\sim 8.49\%$ and that from MT #2 falls by $\sim 21.20\%$. Further, energy procurement from MT #3 and MT #4 fall by $\sim 50\%$ and $\sim 23.93\%$, respectively. The optimal setpoints of the two DCSOPs at each hour are depicted in fig. 2.27. The impact of correlation on the optimal settings of the DCSOPs is negligible in this scenario.

Setpoints of the BESS units for all three scenarios with uncorrelated input RVs are shown in fig. 2.28. Load profiles before and after activating the DR program for the three scenarios are shown in fig. 2.29. The expected OC shows an increasing trend for

the system and input dataset under consideration. At the same time, the loss decreases when the correlation between the input RVs is considered. Further, the above analysis reveals that some optimal setpoints of the flexible resources also change with a correlation between the input RVs.

2.5 Conclusions

An optimal EMS for a grid-connected DCμG is proposed from the perspective of the DCμGO considering the correlation between the uncertain input RVs. Uncertain input RVs are modelled in the probabilistic framework using pdfs. The correlations between the input RVs are incorporated using the inverse NT. The mapping of correlation coefficients from the marginal distributions to the standard normal space is done by a Newton's interpolation method and not by empirical relationships. Therefore, the proposed approach applies to all marginal distributions. The correlated and uncorrelated input RVs are fed to a Hong's 2m PEM algorithm for transferring the uncertainties to output variables. The flexibility coordination model comprises optimal power procurement from the upstream grid, MTs, WPGs, optimal scheduling of BESS and DCSOP, and DR implementation. A convex model of the DCμG is used to obtain guaranteed optimal solutions. A MO optimisation problem is posed with two objectives: cost and loss reduction. The MO optimisation problem is solved using the "epsilon-constraint" algorithm. The proposed EMS is validated by simulation studies on a ten bus DCμG network. The main findings are as follows:

- The expected OC in a day can be minimised up to $\sim 14.31\%$ using the proposed flexibility coordination scheme.

- The expected daily loss can be reduced up to $\sim 1.23\%$.

- When the OC and loss need to be simultaneously reduced, the OC reduces by $\sim 5.80\%$ and the loss decreases by $\sim 1.01\%$.

- DR implementation and BESS scheduling can effectively reduce the OC. However, the impacts of DR and BESS on system loss over a day are insignificant.

- Procuring power from DG units like MTs and WPGs during periods of high loading and high grid energy price can effectively reduce the OC.
- The impact of DCSOP on OC reduction is trivial. However, DCSOP reduces the loss in the network.
- The expected OC increases while the loss reduces when the correlation between the input RVs is considered for the given system. Further, the correlation between input RVs impacts some optimal setpoints of the flexible resources.